Notes on Spin Multipole Graphical Techniques

K. A. Earle

Physics Department, University at Albany (SUNY)

1400 Washington Ave., Albany, NY 12222

December 28, 2008

Abstract

For systems of multiple, coupled spins, a generalization of the Wigner-Eckart theorem to transition (Liouville) space facilitates a concise formulation for the description of spin dynamics. A graphical method introduced by Danos greatly simplifies the trace calculations needed to apply the generalized Wigner-Eckart theorem. One of the intriguing insights that emerges from the graphical analysis is that the trace evaluation decomposes into a modular structure whose individual pieces may be evaluated separately. One may therefore build up a 'library' of intermediate results which may be combined in an intuitive way to describe an arbitrary spin system. In order to demonstrate the very few rules that are required to construct coupled spin graphs and to motivate the utility of the method, two important cases are considered. The first case is an electron (spin S) coupled to a single nucleus (spin I). This case is chosen to facilitate comparison to the uncoupled representation commonly employed in EPR spectral lineshape computations. The second case considered is that of two paramagnetic centers each coupled to a nearby nucleus, for a total of four spins. This case is relevant for macromolecules labeled with two nitroxide spin labels, or other paramagnetic centers interacting via dipole-dipole couplings. The results of these calculations may be conveniently expressed in terms of Wigner 3j, 6j and 9j symbols, for which accurate and efficient methods of computation exist.

1 Introduction

Density matrix methods play an important role in the computation of spin dynamics. For systems that can be described by only one or two relevant spins, it is a straightforward, though tedious, exercise to work with the spin operators directly in an uncoupled basis. This is the approach developed by Pyper[1] and applied by Freed and co-workers in their classic analysis of the EPR lineshape problem.[2] In that calculation, angular momentum theory was used to systematize and organize those aspects of the computation involving spatial degrees of freedom for the relevant relaxation mechanism, rotational diffusion. The relevant basis set describing the spin operators in transition (or Liouville) space did not take advantage of the precision and economy of notation achievable by representing the spin basis set in terms of coupled Irreducible Spherical Tensor Operators (ISTO's) as advocated by Sanctuary and coworkers.[6] Nevertheless, the expressions for the matrix elements that one derives in the uncoupled basis are extremely useful and have been applied to the analysis of a wide variety of systems over the years. Recent reviews of applications of these methods to the high field EPR case are available elsewhere.[3, 4]

Although the bottom-up approach developed by Freed and co-workers is constructive and useful, extensions of the formalism require recomputation from scratch. Examination of the expressions for the relevant matrix elements [2, 5] may convince the reader that a more general, top-down approach would be valuable for extensions of the theory to situations of greater complexity, although it should be stressed that results obtained *via* different methods must be equivalent physically. The question is, rather, one of the *insights* that one may obtain by comparison of different approaches. In addition, the proper choice of basis set can reduce the computational burden, as a basis that is a more faithful representation of the underlying spin dynamics will lead to smaller matrix representations of the relevant equations of motion.

Since Racah's pioneering work in the 40's on the theory of complex spectra,[7] tensor operator methods have become an increasingly indispensable tool for the study of spin dynamics. Just as Judd's classic text on operator techniques [8] made the insights of Racah and others more accessible to atomic spectroscopists, the book by Blum [9] provided a usable textbook for learning how to apply tensor operator techniques in the study of spin dynamics. Traditional methods of evaluation,

based on algebraic manipulations of sums over azimuthal magnetic quantum numbers in products of vector coupling coefficients, lead to expressions with an evident structure, but no obvious insight into how the results may be extended to more complicated cases, or reduced to simpler forms when spins decouple.

One also notes that although the algebraic approach typically requires sums over intermediate azimuthal magnetic quantum numbers, these ancillary quantities do not appear in the final expressions. This observation suggests that a method of evaluation based on coordinate-free, invariant quantities would greatly simplify the required calculations. One may then represent dependencies among the invariant quantities by graphical means. This approach was developed by Jucys and co-workers.[10] El Baz and Castel presented a modified version of the graphical methods of Jucys with useful extensions of the method.[11]

The notion of a graphical representation is very appealing in that the structure may be evaluated piece-wise and a library of analytical expressions for spin coupling 'modules' can be built up. By drawing a suitable graph and identifying the contributions from the invariant modules, one may reuse results of prior calculations and construct expressions for arbitrary spin systems. This mechanism of modular dependence and reuse will be familiar to practitioners of object-oriented programing (OOP) and can serve as a basis for an angular momentum calculation graphical user interface (GUI).

Although the graphical techniques pioneered by Jucys[10] have been available to facilitate angular momentum calculations for some time, their use in this author's experience requires great care in order to achieve consistent phases due to the plethora of oriented line segments and nodes attendant on the method. Another disadvantage of the graphical methods of Jucys, in this author's opinon, is that the recoupling manipulations cause profound changes to the appearance of the diagram, and it can be difficult to reconstruct intermediate steps.

Danos developed an alternative graphical technique which displays the recouplings in a form reminiscent of a flow chart or a circuit schematic.[12] Danos' methods restrict the phase by always working with contrastandard tensors. Where costandard tensors appear, they are re-expressed in terms of contrastandard quantities. An example of this procedure may clarify matters.[11, 13] Kets

transform under rotations in contrastandard fashion, *i.e.*

$$|JN\rangle' = \sum_M |JM\rangle \mathcal{D}^J_{MN}(R). \tag{1}$$

The states conjugate to kets (bras) transform as costandard tensors

$$\langle JN|' = \sum_M \left(\mathcal{D}^J_{MN}(R)\right)^* \langle JM| \tag{2}$$

There is a one-to-one correspondence between the two sets, even though they reside in spaces dual to one another. This implies the existence of a metric which can be related to the Clebsch-Gordan coefficients coupling two tensors to a rank zero tensor. Silver's book may be consulted for an elementary account of the issues involved as well as a physical plausibility argument for the connection between the adjoint operation and time reversal symmetry.[15] A detailed exposition of the relevant mathematics from the perspective of a physicist is given by Nakahara.[16] The U matrix of Fano and Racah fills the same role in changing the gredience of the tensors under study.[14] With due regard for the required mathematical hygiene, the result is that kets and bras may be put into a one-to-one correspondence, *i.e.*

$$\langle JM| = (-)^{J-M}|J\,-M\rangle, \tag{3}$$

where the reader is reminded that Equation 3 only has meaning because the dual spaces of bras and kets are related by a metric.

As Brink and Satchler note,[13] the 'extra' factor of $(-)^J$ is arbitrary, but it does allow one to express products of tensor operators as quantities with simple transformation properties under the time reversal operation. This is related to the K symmetrization operation for general matrix elements of the Stochastic Liouville Equation, as will be seen. The basis used here corresponds to the following phase convention for the q components of a rank k tensor operator

$$\begin{aligned} T_{kq} &= (-)^{k-q} T^\dagger_{k\,-q}, \text{or} \\ T^\dagger_{kq} &= (-)^{k+q} T_{k\,-q} \end{aligned} \tag{4}$$

This is the choice advocated by Danos. By consistent adherence to this convention, one need not use oriented lines or nodes in a graphical approach, as will be seen. This simplification reduces

the opportunities for phase errors. The astute reader will have realized that this choice of phase does require certain changes in handling well-established quantities, such as spherical harmonics. In general, $\left(Y_m^l\right)^* = (-)^{-m} Y_{-m}^l$ which does not obey the phase convention of Danos. The following quantities *do* obey Danos' convention $\mathcal{Y}_m^l = (-i)^l Y_m^l$. While not as common as the conventional spherical harmonics, the $\{\mathcal{Y}\}$ do have advantages for tensorial algebra applications and also for related considerations under the time reversal operator.[14, 15] Some readers may be familiar with the set of spherical harmonics $\mathfrak{Y}_m^l = (i)^l Y_m^l$ which uses a different phase convention than Danos' phase convention.[12] The 'extra' factor of $(-)^l$ is explained in Danos.[12] It corresponds to the folowing choice of spherical basis

$$\begin{aligned} e_1^{[1]} &= \frac{i}{\sqrt{2}} \left(\hat{e}_x + i\hat{e}_y\right) \\ e_0^{[1]} &= -i\hat{e}_z \\ e_{-1}^{[1]} &= -\frac{i}{\sqrt{2}} \left(\hat{e}_x - i\hat{e}_y\right) \end{aligned} \tag{5}$$

where the 'square bracket' notation indicates that the basis vectors transform contragrediently.[14] This point is discussed more fully in Section 6.

After Danos' initial publication, an NBS report by Lehmann and O'Connell provided a pedagogical explication of Danos' method.[17] A more complete treatment, with further refinements and extensions of Danos' graphical methods, was finally given by Danos and Gillet.[18] The theoretical background necessary for understanding the phase choice of the graphical method is discussed in Fano and Racah.[14] The result of applying Danos' methods is a recoupling diagram from which one may simply read off an analytical expression in terms of amplitudes, phases and Wigner 3nj symbols. In practice, only 3j, 6j and 9j symbols are needed for analytical work. Python modules, based on a Maple implementation of Racah's analytical expressions,[19] are available for numerical evaluation of the required 3nj symbols.[20] Except for Danos' original paper,[12] expositions of his invariant graph technique are published in obscure or difficult to find form. In an effort to make these techniques more widely known, the author will present a précis of Danos' invariant graph method.

2 Invariant Graphs

The fundamental object in the invariant graph method is the vector coupling coefficient for four angular momenta, which is proportional to a 9j symbol.[21, 22] Suppose that the original couplings may be expressed as $a + b \rightarrow e$, $c + d \rightarrow f$ and $e + f \rightarrow i$. If the recouplings are expressed as $a + c \rightarrow g$, $b + d \rightarrow h$ and $g + h \rightarrow i$, then one can represent the required vector coupling coefficient in terms of the following nine entry tableau[1]

$$\left[\begin{array}{ccc} a & b & e \\ c & d & f \\ g & h & i \end{array} \right] = \sqrt{2e+1}\sqrt{2f+1}\sqrt{2g+1}\sqrt{2h+1} \left\{ \begin{array}{ccc} a & b & e \\ c & d & f \\ g & h & i \end{array} \right\} \tag{6}$$

The quantity on the right hand side of Equation 6 in curly brackets is a Wigner 9j symbol. The normalization of the square bracket box is chosen to simplify as far as possible manipulation of the recouplings, as will be seen in the sequel. In order to reduce notational clutter, it is conventional in the invariant graph method to define the ubiquitous square root factors $\sqrt{2j+1}$ as

$$\sqrt{2j+1} \equiv \hat{\jmath}. \tag{7}$$

Equation 7 will be used to simplify the presentation of many invariant diagrams. It will also be used to simplify final analytical expressions as well. The square bracket box in Equation 6 has the graphical representation shown in Figure 1. In any invariant coupling diagram, when this box occurs, it may be replaced by its analytical expression Equation 6. In order to avoid carrying complicating amplitude factors in angular momentum calculations, Danos and Gillet recommend using the square bracket form of the recoupling diagram.[18] In order to compare with expressions in the literature, one may of course rewrite recoupling diagrams in terms of Wigner 9j symbols and the appropriate amplitude factors. When one of the angular momenta in the recoupling diagram is zero, one may replace the relevant line in Figure 1 with a dashed line.[18] For this special case, the square bracket invariant degenerates into the product of a phase, an amplitude factor and a Wigner 6j symbol (or Racah W symbol). All possible cases are discussed in Danos and Gillet.[18] When two or three momenta vanish the resulting analytical expression for a square bracket symbol

[1] See Biedernharn and Louck, pp. 458–459.[22]

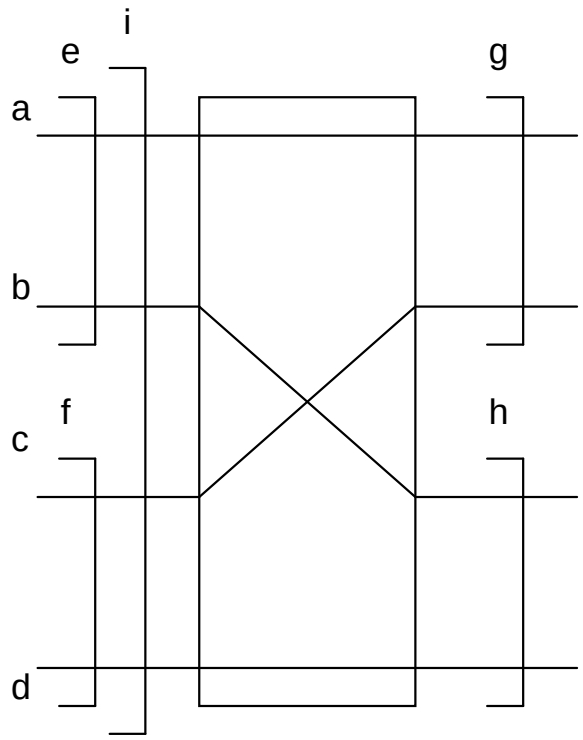

Figure 1: The invariant recoupling diagram of four angular momenta. This diagram has an analytical realization in terms of a vector coupling coefficient, or a Wigner 9j symbol (Racah X symbol) times a normalization constant. See the text for more details.

is the product of a phase and an amplitude. For convenience, the table of Danos and Gillet[18] is reproduced in Appendix A.

As an example of the utility of the graphical method, one may prove the following identity by graphical means

$$\left\{ \begin{array}{ccc} a & b & e \\ c & d & f \\ g & h & i \end{array} \right\} = \sum_l (-)^{2l} (2l+1) \left\{ \begin{array}{ccc} a & c & g \\ l & b & d \end{array} \right\} \left\{ \begin{array}{ccc} b & d & h \\ i & g & l \end{array} \right\} \left\{ \begin{array}{ccc} e & f & i \\ d & l & c \end{array} \right\} \tag{8}$$

A graphical proof of Equation 8 using the techniques of Jucys is given in Appendix B. To prove the identity in Equation 8 by resolutely pedestrian algebraic means, requires the evaluation of an interlocking sum over 18 azimuthal magnetic quantum numbers, subject to constraints, appearing in the product of six 3j symbols and applying various identities for 6j symbols. This procedure is

carried out in Appendix C but it is hardly an intuitive approach, and it is fraught with opportunities for making mistakes in evaluating the proper phase and amplitude. Of course, a judicious choice in the method of organizing the evaluation of the sum can make the job easier, but given that none of the azimuthal magnetic quantum numbers appear in the final result a method of evaluation that dispenses with them entirely would be preferable. As an example of this perspective, Biedenharn and Louck give a symbolic derivation of this result that is independent of the underlying Wigner coefficient structure.[2] In Biedenharn and Louck's formulation, the required recouplings take the following form

$$[(ac)_g(bd)_h]_i \xrightarrow{R} \{[(ac)_g b]_l d\}_i \xrightarrow{\phi} \{[b(ac)_g]_l d\}_i \xrightarrow{R,\phi} \{[(ab)_e c]_l d\}_i \xrightarrow{R} [(ab)_e(cd)_f]_i. \tag{9}$$

Here, the stacked relation operator keeps track of Racah W coefficients (6j symbols) due to associative recouplings and phase terms due to tensor reorderings, *e.g.*, $(ab)_e = (-)^{a+b-e}(ba)_e$. Although this chain of transformations achieves great economy of notation, this author finds that the recouplings are still difficult to visualize clearly.

A graphical proof of Equation 8 using the methods of Danos and Gillet is shown in Figure 2.[18] In analytical form, the graph in Figure 2 reads as follows

$$\begin{bmatrix} a & b & e \\ c & d & f \\ g & h & i \end{bmatrix} = \sum_l \begin{bmatrix} e & 0 & e \\ c & d & f \\ l & d & i \end{bmatrix} \begin{bmatrix} a & b & e \\ c & 0 & c \\ g & b & l \end{bmatrix} \begin{bmatrix} g & b & l \\ 0 & d & d \\ g & h & i \end{bmatrix}. \tag{10}$$

$$= \sum_l \begin{bmatrix} d & c & f \\ 0 & e & e \\ d & l & i \end{bmatrix} \begin{bmatrix} 0 & c & c \\ b & a & e \\ b & g & l \end{bmatrix} \begin{bmatrix} d & 0 & d \\ b & g & l \\ h & g & i \end{bmatrix} \tag{11}$$

Equations 10 and 11 are equivalent due to the identities of Danos and Gillet,[18] given in Appendix A. The equations refer to different, equivalent methods of performing the recoupling, as may be seen by comparing the diagrammatic approach given here to the approaches given in the

[2] *ibid.*, pg. 457

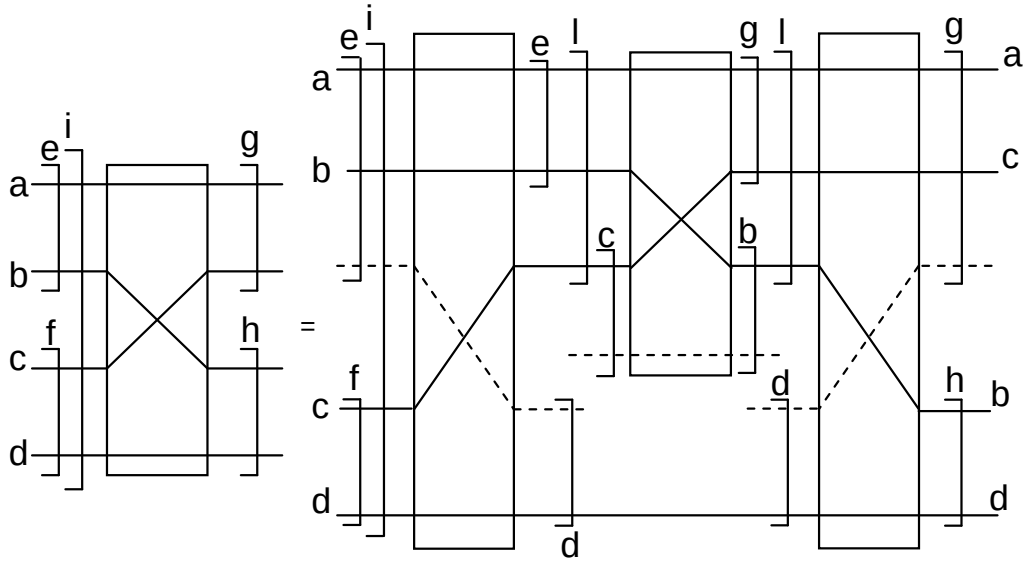

Figure 2: This is a graphical representation of the identity given in Equation 8. Note that a dashed line indicates a zero angular momentum line. In the graphical method, intermediate angular momenta, such as l in this case, are summed over. All other indices are fixed in this graph.

appendices. The result may be expressed in terms of 9j and 6j symbols as follows

$$\hat{e}\hat{f}\hat{g}\hat{h}\begin{Bmatrix} a & b & e \\ c & d & f \\ g & h & i \end{Bmatrix} =$$

$$\sum_l (-)^{i+c+e+d}\hat{l}\hat{f}\begin{Bmatrix} i & l & d \\ c & f & e \end{Bmatrix}(-)^{g+e+c+b}\hat{g}\hat{e}\begin{Bmatrix} l & g & b \\ a & e & c \end{Bmatrix}(-)^{i+b+d+g}\hat{h}\hat{l}\begin{Bmatrix} g & h & i \\ b & l & d \end{Bmatrix}. \quad (12)$$

Equation 12 may be rewritten as Equation 8 by using the symmetries of the 6j symbols under interchange of columns and interchange of row entries in any two columns.[13] The phase may be simplified by exploiting the observation that certain sets of 6j symbol entries satisfy the triangle rule, *e.g.*, $2(i+d+l)$ must be an even integer and four times any single index must be an even

integer.[13] It should be noted that the symmetries of the Wigner 6j and 9j symbols allow one to rewrite the identity in Equation 8 in a variety of ways that may not appear to be equivalent on casual inspection. Expressing all quantities in terms of recoupling boxes and applying the identities in Appendix A allows one to see the equivalence of various forms more easily.

3 Spin Operator Invariants

3.1 Notational Features

At this point, it is useful to enquire more thoroughly after the nature of the input and output lines appearing in Figure 1. Two lines bracketed together with a square bracket, *e.g.*, lines a and b bracketed by e in Figure 1 refer to a tensor product $\left[\psi^{[a]}\phi^{[b]}\right]^{[e]}$ in the notation of Fano and Racah,[14] or an oriented node in the diagrammatic approach of Jucys as extended by El Baz and Castel.[10, 11] Note that the azimuthal magnetic quantum numbers are not explicitly indicated. This object can be used to represent, *e.g.*, a ket $|\psi\rangle \otimes |\phi\rangle$ in a product basis. In order to define a bra, one must have a consistent description for the effect of the adjoint operation. This will be addressed more fully below. The full notation for this object is

$$\left[\psi^{[a]}\phi^{[b]}\right]^{[e]} \equiv \left[\psi^{[a]}\phi^{[b]}\right]^{[e]}_{m_e} = \sum_{m_a,m_b} (a\, b\, m_a\, m_b | e\, m_e)\, \psi^{[a]}_{m_a}\phi^{[b]}_{m_b} \tag{13}$$

Invariants that do not explicitly depend on azimuthal quantum numbers will be used as much as possible. The invariant graph method implicitly assumes sums over azimuthal quantum numbers so they need never be displayed, except when information about how the system is prepared and observed is explicitly required. The quantity in round brackets is a vector coupling or Clebsch-Gordan coefficient. The square brackets indicate that the tensor quantities transform as contragredient (or contrastandard) tensors.[14, 18] For a given active transformation parameterized by Ω, contragredient tensors transform as

$$\psi'^{[I]}_{M'} = \sum_{M=-I}^{M=I} \psi^{[I]}_{M}\mathcal{D}^{I}_{MM'}(\Omega). \tag{14}$$

in the notation of Danos and Gillet.[18] Fano and Racah[14] define contrastandard tensors that transform under *passive* transformations as

$$\psi'^{[I]}_{M'} = \sum_{M=-I}^{M=I} \mathcal{D}^{I}_{M'M}(\Omega)^{*} \psi^{[I]}_{M}. \tag{15}$$

This form is useful for transforming magnetic tensor components from a body-fixed coordinate system to a space or lab fixed coordinate system.

3.2 Invariants of rank 0

The invariant object $\left[\tilde{A}^{[I]} B^{[J]}\right]^{[0]}$ is particularly important in invariant graph theory. The tilde indicates the transpose operation if the tensorial quantities have spinor character. Using the symmetries of the vector coupling coefficients, this invariant may be written

$$\left[\tilde{A}^{[I]} B^{[J]}\right]^{[0]} = \sum_{M} (I\, I\, -M\, M|0\, 0) \tilde{A}^{[I]}_{-M} B^{[I]}_{M} = \frac{1}{\hat{I}} \sum_{M} (-)^{I+M} \tilde{A}^{[I]}_{-M} B^{[I]}_{M} \tag{16}$$

One may use the final form of Equation 16 to define an adjoint operator in the contragredient space

$$\left[\tilde{A}^{[I]} B^{[J]}\right]^{[0]} \equiv \frac{1}{\hat{I}} \sum_{M} \left(A^{[I]}_{M}\right)^{\dagger} B^{[I]}_{M} \tag{17}$$

where

$$\left(A^{[I]}_{M}\right)^{\dagger} \equiv (-)^{I+M} \tilde{A}^{[I]}_{-M} \tag{18}$$

As noted by Danos and Gillet, this choice for the adjoint operator allows one to always work with contragredient tensors, which is one of the considerations that immensely simplifies the bookkeeping associated with ensuring the proper phase.[18] Note that this representation of the adjoint is similar to the transformation between bras and kets given in Equation 3. Just as for Equation 3, Equation 18 only makes sense given the existence of a metric defined by the Clebsch-Gordan coefficients. The choice of phase implied by Equation 18 is equivalent to the one used by Sanctuary and co-workers in their work on multipole operators with many applications in NMR.[6] This work will build on the multipole operator formalism by recasting it in a graphical form that displays the angular momentum recouplings in a straightforward way.

3.3 Multipole Operator Basis

A multipole operator may be written in the following form

$$\mathcal{Q}_{\sigma}^{[\Sigma]} = (-i)^{\Sigma} \sum_{n,n'} (S\, S\, n\, -n'|\Sigma\, \sigma) \Psi_{n}^{[S]} \tilde{\Psi}_{-n'}^{[S]}. \tag{19}$$

This may be rewritten in terms of the adjoint operator by introducing a factor of unity written as $(-)^{2(S+n')}$. Thus

$$\begin{aligned} \mathcal{Q}_{\sigma}^{[\Sigma]} &= (-i)^{\Sigma} \sum_{n,n'} (S\, S\, n\, -n'|\Sigma\, \sigma)(-)^{S+n'} \Psi_{n}^{[S]} \left(\Psi_{n'}^{[S]} \right)^{\dagger} \\ &\equiv (-i)^{\Sigma} \sum_{n,n'} (S\, S\, n\, -n'|\Sigma\, \sigma)(-)^{S+n'} |S, n\rangle\langle S, n'|. \end{aligned} \tag{20}$$

This notation shows the equivalence between the irreducible tensorial set representation of Fano and Racah[14] and the Dirac representation in terms of bras and kets. In order to facilitate comparison of these operators with forms already in the literature, one may rewrite the vector coupling coefficient in terms of a 3j symbol, *viz.*

$$(S\, S\, n\, -n'|\Sigma\, \sigma) = (-)^{\sigma} \hat{\Sigma} \begin{pmatrix} S & S & \Sigma \\ n & -n' & -\sigma \end{pmatrix}. \tag{21}$$

With this notation, the $\mathcal{Q}$ operators may be written in the form

$$\mathcal{Q}_{\sigma}^{[\Sigma]} = (-i)^{\Sigma} \hat{\Sigma} \sum_{n,n'} (-)^{S+n} \begin{pmatrix} S & S & \Sigma \\ -n & n' & \sigma \end{pmatrix} |S, n\rangle\langle S, n'| \tag{22}$$

This set is the same as the one used by Sanctuary.[6] One may use the symmetries of the 3j symbol in Equation 22 to verify this. This set of operators is similar to the $Q^{(\Sigma,\sigma)}(S)$ operators used by Benetis [24] and also by Kruk [25] which satisfy the conventional phase relation $\left(Q^{(\Sigma,\sigma)}(S)\right)^{\dagger} = (-)^{\sigma} Q^{(\Sigma,-\sigma)}(S)$. Thus the basis sets of Benetis and Kruk have different invariance properties than the $\mathcal{Q}$ operators considered here. In order to preserve the useful invariance properties of Danos' $\mathcal{Q}$ operators, $\{\mathcal{Q}\}$ will be used for all calculations presented here. Some examples may aid the reader in learning how to manipulate the $\{\mathcal{Q}\}$. In section 3.4, as a mnemonic device, operators that obey the standard phase convention will be given in italics. Operators that obey Danos' phase convention will be shown in a calligraphic font.

3.4 Multipole Operator Invariants

In order to use multipole operators within the context of the invariant graph method, it is necessary to couple the $\mathcal{Q}$ operators to an irreducible tensor of the same rank, such that the tensor product of the $\mathcal{Q}$ operators and the complementary irreducible tensorial set transform as a tensor of rank 0 under coordinate transformations (*i.e.*, as a scalar). One may define a weight tensor which is constructed to select a particular, desired multipole order from the following invariant object

$$\left[\tilde{\mathcal{W}}^{[\Sigma]}\mathcal{Q}^{[\Sigma]}\right]^{[0]} = \sum_{\sigma'}(\Sigma\Sigma - \sigma'\sigma'|00)\tilde{\mathcal{W}}^{[\Sigma]}_{-\sigma'}\mathcal{Q}^{[\Sigma]}_{\sigma'}, \tag{23}$$

where the $\mathcal{W}$ tensor is a normalized tensor such that

$$\sum_{\sigma'}\left(\mathcal{W}^{[\Sigma]}_{\sigma'}\right)^{\dagger}\mathcal{W}^{[\Sigma]}_{\sigma'} = 1. \tag{24}$$

Note that with this definition of $\mathcal{W}$ there is still an arbitrary choice of phase. One may exploit this freedom to ensure that matrix elements have a particular behavior under complex conjugation, for example. This phase freedom will be used to express matrix elements computed by invariant means in a form that can be compared more easily with previously published expressions, as shown below.[6]

In terms of the adjoint operation, Equation 23 may be rewritten as follows

$$\left[\tilde{\mathcal{W}}^{[\Sigma]}\mathcal{Q}^{[\Sigma]}\right]^{[0]} = \frac{1}{\hat{\Sigma}}\sum_{\sigma'}\left(\mathcal{W}^{[\Sigma]}_{\sigma'}\right)^{\dagger}\mathcal{Q}^{[\Sigma]}_{\sigma'} \tag{25}$$

A given operator $\mathcal{Q}$ may thus be written in invariant form as follows

$$\begin{aligned}\mathcal{Q}^{[\Sigma]}_{\sigma} &\equiv \sum_{\sigma'}\left(\mathcal{W}^{[\Sigma]}_{\sigma'}\right)^{\dagger}\mathcal{Q}^{[\Sigma]}_{\sigma'} \\ &= \hat{\Sigma}\left[\tilde{\mathcal{W}}^{[\Sigma]}\mathcal{Q}^{[\Sigma]}\right]^{[0]} \\ &= \hat{\Sigma}\left[\mathcal{W}^{[\Sigma]}\mathcal{Q}^{[\Sigma]}\right]^{[0]},\end{aligned} \tag{26}$$

where the observation that the weight tensor does not have spinor character has been used to remove the tilde. This is a handy notational convenience as it allows one to distinguish weight tensors that arise from operators that transform as kets. Note that in this application, the weight tensor can be used to project out a $\mathcal{Q}$ operator with a specific azimuthal quantum number. One

can use this property of the weight tensor to recast matrix element calculations of specific operators in invariant form, as will be shown.

The invariant expression for an adjoint operator may be written as follows

$$\left(\mathcal{Q}_{\sigma}^{[\Sigma]}\right)^{\dagger} \equiv \hat{\Sigma}\left[\tilde{\mathcal{W}}^{[\Sigma]}\tilde{\mathcal{Q}}^{[\Sigma]}\right]^{[0]}. \tag{27}$$

Here, the tildes indicate that both the weight tensor and the transition space state vector Q originate from a bra in transition state space. In order to simplify the notation somewhat, the convention will now be that all operators, regardless of typeface, satisfy Danos' phase convention, unless explicitly stated otherwise.

In order to check that the transition space Q vectors are properly normalized, it is necessary to construct a rank 0 invariant from the weight tensors and from the Q vectors. The rank 0 invariant constructed from the W tensor and its adjoint has the following value

$$\left[\tilde{W}^{[\Sigma]}W^{[\Sigma]}\right]^{[0]} = \frac{1}{\hat{\Sigma}}, \tag{28}$$

when the normalization condition Equation 24 is used. If one considers the Q operator to be a state vector Ψ in transition space, the proper normalization is

$$\int d\tau \left(\Psi_{\sigma}^{[\Sigma]}\right)^{\dagger} \Psi_{\sigma}^{[\Sigma]} = 1. \tag{29}$$

If all of the states are normalized, then the invariant constructed from the $2\Sigma + 1$ normalized state vectors is

$$\left[\tilde{\Psi}^{[\Sigma]}\Psi^{[\Sigma]}\right]^{[0]} = \frac{\hat{\Sigma}^2}{\hat{\Sigma}} = \hat{\Sigma} \tag{30}$$

The norm of a state vector Q is typically computed as follows

$$\langle Q_{\sigma}^{[\Sigma]} | Q_{\sigma}^{[\Sigma]} \rangle = \int d\tau \left(Q_{\sigma}^{[\Sigma]}\right)^{\dagger} Q_{\sigma}^{[\Sigma]} = \int d\tau \hat{\Sigma}\left[\tilde{W}^{[\Sigma]}\tilde{Q}^{[\Sigma]}\right]^{[0]} \hat{\Sigma}\left[W^{[\Sigma]}Q^{[\Sigma]}\right]^{[0]} \tag{31}$$

In order to take advantage of the normalization conditions expressed by Equations 28 and 30 it is necessary to recouple the invariants in Equation 31. This can be accomplished using the vector coupling coefficient in Equation 6. The process may be represented by the graph shown in Figure 3. The analytical form of Figure 3 may be read off the graph as follows

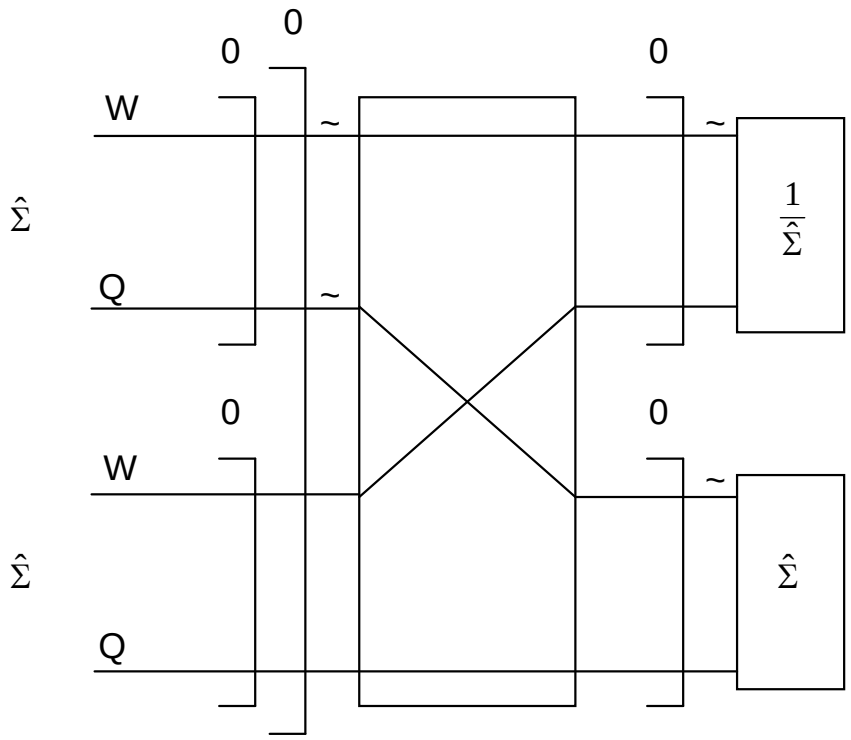

Figure 3: The invariant recoupling diagram of four angular momenta appearing in the state normalization integral of Equation 31. The invariant norms $\hat{\Sigma}$ and $1/\hat{\Sigma}$ are shown in terminal boxes corresponding to Equations 28 and 30. See the text for more details.

$$\langle \Sigma, \sigma | \Sigma, \sigma \rangle = \hat{\Sigma}\hat{\Sigma} \begin{bmatrix} \Sigma & \Sigma & 0 \\ \Sigma & \Sigma & 0 \\ 0 & 0 & 0 \end{bmatrix} \frac{1}{\hat{\Sigma}} \hat{\Sigma}, \tag{32}$$

where the factors are read off top to bottom and left to right. The vector coupling box has the value $\hat{0}/(\hat{\Sigma}\hat{\Sigma})$ and so the analytical expression for the normalization integral becomes

$$\langle \Sigma, \sigma | \Sigma, \sigma \rangle = \hat{\Sigma}\hat{\Sigma} \frac{\hat{0}}{\hat{\Sigma}\hat{\Sigma}} \frac{1}{\hat{\Sigma}} \hat{\Sigma} = \hat{0} = 1. \tag{33}$$

Thus, the Q states are normalized. The rules for constructing this invariant graph may be summarized as follows: the first step is to construct the state invariants $[W^{[\Sigma]}Q^{[\Sigma]}]^{[0]}$ corresponding to a ket and $[\tilde{W}^{[\Sigma]}\tilde{Q}^{[\Sigma]}]^{[0]}$ corresponding to a bra. Each state invariant contributes a factor $\hat{\Sigma}$ which is placed to the left of the invariant graph. It is conventional to place invariants originating from bras

above invariants originating from kets. The provenance of the invariant is indicated by labeling lines originating from bra invariants with tildes. Vector coefficient recoupling boxes are used to recouple tensors so they may be combined in invariant norms at the right hand side of the graph. The convention is that the tilde lines enter the top of the invariant norm boxes. Each weight norm contributes a factor of $1/\hat{\Sigma}$. Each state norm contributes a factor $\hat{\Sigma}$. The analytical expression for the graph is determined by multiplying all the prefactors, recoupling box values and invariant norm factors together.

3.5 Evaluation of Trace Norms

Although the norm calculation was done in transition space, where the Q tensors were treated as states, it is useful to have a formalism for computing the trace norm in state space where the Q tensors are treated as operators. The trace norm may be written as follows

$$\begin{aligned} \langle \Sigma, \sigma | \Sigma, \sigma \rangle &= Tr \left\{ \left(Q_\sigma^{[\Sigma]} \right)^\dagger Q_\sigma^{[\Sigma]} \right\} \\ &\equiv \sum_{m_S} \langle m_S | \left(Q_\sigma^{[\Sigma]} \right)^\dagger Q_\sigma^{[\Sigma]} | m_S \rangle \end{aligned} \tag{34}$$

The graphical representation of Equation 34 will afford the opportunity of introducing a new recoupling diagram which will keep track of internal phase changes as tensors are reordered in order to allow couplings to terminate in invariant norms. It is a special case of the recoupling diagram shown in Figure 1 where the lines a and d have angular momentum 0. In that case, the recoupling box has the value $(-)^{b+c-i}$ using the labeling of Figure 1, *i.e.*,

$$\begin{bmatrix} 0 & b & b \\ c & 0 & c \\ c & b & i \end{bmatrix} = (-)^{b+c-i} \tag{35}$$

In this case, the two zero momentum lines are 'spectator' lines and are typically omitted leaving a recoupling box with two crossed lines, or groups of crossed lines, if it is informative or necessary to keep track of internal couplings.

The diagram appropriate to Equation 34 is shown in Figure 4. There are a number of noteworthy features in this diagram that will have consequences for evaluating traces of operator products. One

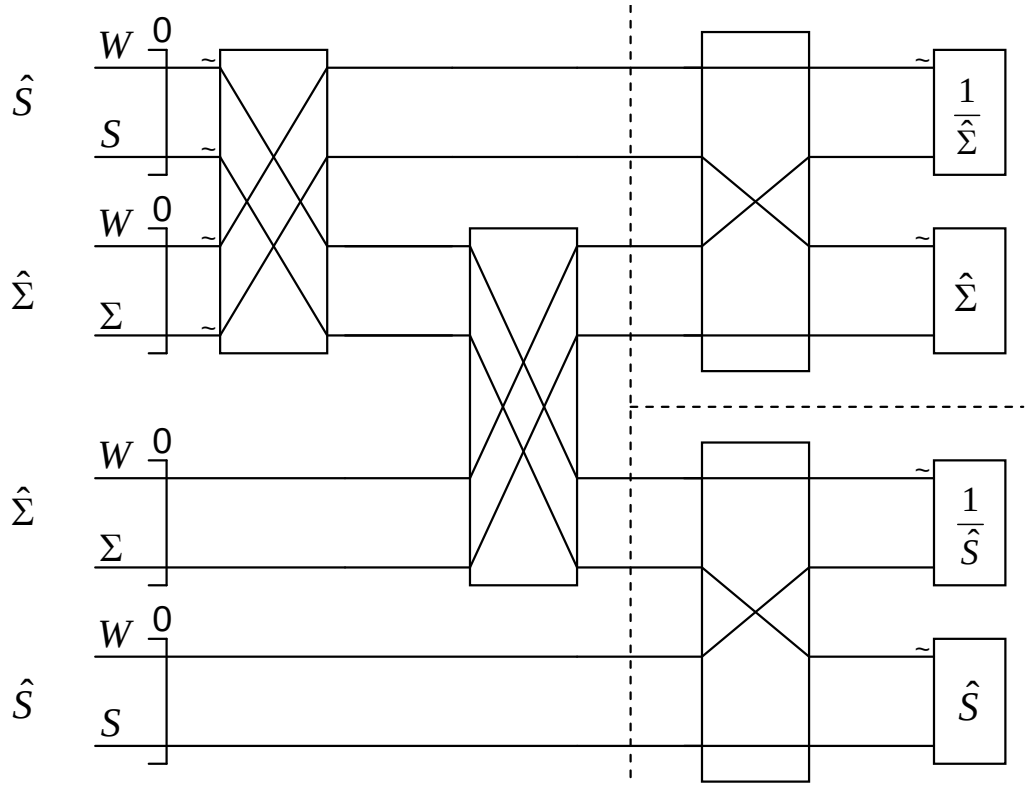

Figure 4: This figure shows the invariant diagram for the trace norm where the Q tensors are treated as operators in state space. The dashed lines indicate subgraphs that are equivalent to graphs for which analytical expressions have already been given. The identification of the subgraphs with previously derived results is the first example of the 'modular' nature of the invariant graph technique. See the text for more details.

important point is that the S tensor lines 'cascade' through the Q operator lines and terminate in a subgraph of the form of Figure 3. This is a consequence of the trace operation defined in Equation 34. This subgraph cancels the prefactors of $\hat{S}\hat{S}$ in Figure 4 due to the recoupling box so that the remaining subgraph is identical to that originally evaluated in Figure 3.

The analytical expression corresponding to the graph in Figure 4 is

$$\hat{S}\hat{\Sigma}\hat{\Sigma}\hat{S}(-)^{0+0-0}(-)^{0+0-0}\begin{bmatrix}\Sigma & \Sigma & 0\\ \Sigma & \Sigma & 0\\ 0 & 0 & 0\end{bmatrix}\begin{bmatrix}S & S & 0\\ S & S & 0\\ 0 & 0 & 0\end{bmatrix}\frac{1}{\hat{\Sigma}}\hat{\Sigma}\frac{1}{\hat{S}}\hat{S}=1 \tag{36}$$

Put another way, Figure 4 provides a graphical proof of the *physical* equivalence of the trace norm

where the Q tensors are treated as operators in state space and the state norm where the Q tensors are treated as states in transition space. This proof obtains because the product of the recoupling phases on the left hand side of Figure 4 are unity. Danos and Gillet discuss the modifications to the invariant graph method that are necessary when one is operating in a Fock space where the invariant tensors involve creation and annihilation operators.[18]

It is useful to note that the S lines in Figure 4 are 'spectator lines' and one may omit or retain them according to personal preference. They do not affect the final result. In order to simplify invariant diagrams corresponding to multiple coupled spins, the 'spectator' lines in the trace norm will be omitted.

4 Spin Multipole Matrix Elements

The spin dyamics of a system is governed by the Liouville von Neumann equation

$$\frac{\partial \rho}{\partial t} = -\frac{i}{\hbar}\left[\mathcal{H}, \rho\right] \equiv -\frac{i}{\hbar}\mathcal{H}^{\times}\rho \tag{37}$$

From a mathematical perspective, Equation 37 may be viewed as a mapping of the spin density matrix at time t_i, which may be expanded in a complete set of spin multipoles, to the spin density matrix at some infinitesimally later time t_f, which may be expanded in the same complete set of spin multipoles. The Hamiltonian corresponding to the mapping may also be expressed in terms of the same complete set of spin multipoles. The matrix elements of the mapping may be expressed by the following trace operation

$$\langle \rho_f | - \frac{i}{\hbar}\mathcal{H}^{\times}|\rho_i\rangle \propto Tr\left\{\left(Q_{\sigma''}^{[\Sigma'']}\right)^{\dagger}\left[Q_{\sigma'}^{[\Sigma']}, Q_{\sigma}^{[\Sigma]}\right]\right\}. \tag{38}$$

The invariant graph method will be used to evaluate the trace in Equation 38. Evaluating the trace of products of more than two tensors will introduce some new graphs, whose physical content can be quickly summarized as an instance of a generalized Wigner-Eckart theorem, suitable for traces of operators.

An invariant graph corresponding to one 'half' of the commutator relation in Equation 38 is shown in Figure 5. The other 'half' may be obtained by a trivial reordering of the Q operators in

Figure 5 and taking the appropriate difference. The effect of these operations will be discussed in more detail below. As discussed in Section 3.5, one may omit the 'spectator' lines as they merely contribute a factor of unity for properly normalized states. The analytical form of this graph may

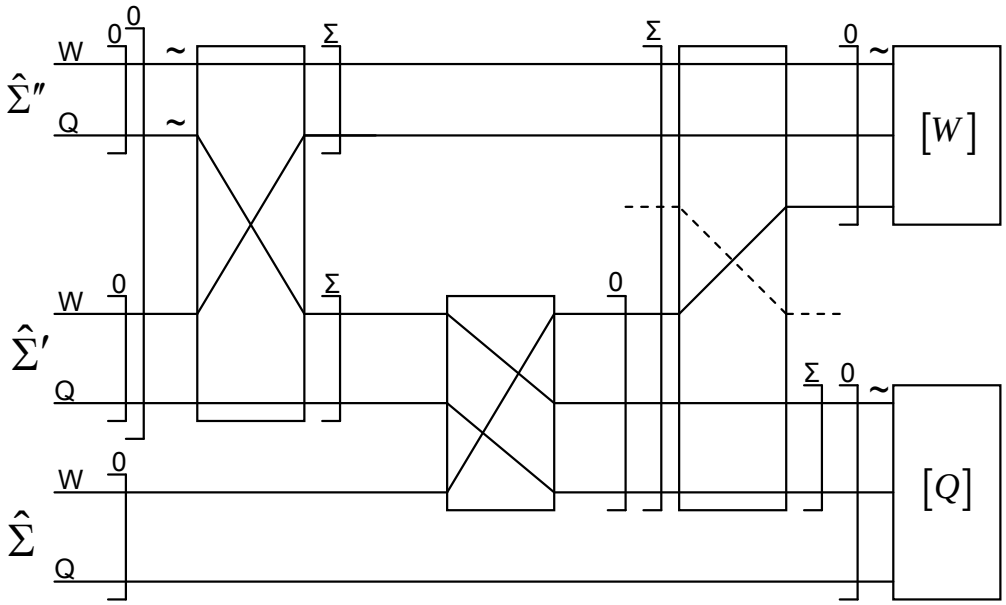

Figure 5: This figure shows the invariant diagram for the trace of three Q tensors. It is a graphical statement of the Wigner-Eckart theorem. The terminal box containing the $[W]$ symbol is proportional to a single Wigner 3j symbol or vector coupling coefficient if the azimuthal quantum numbers of the three Q tensors are specified. The terminal box containing the Q symbol is a reduced matrix element. It can be evaluated by invariant means. See the text for more details.

be written explicitly as

$$Tr\left\{\left(Q_{\sigma''}^{[\Sigma'']}\right)^{\dagger} Q_{\sigma'}^{[\Sigma']} Q_{\sigma}^{[\Sigma]}\right\} =$$

$$\hat{\Sigma}''\hat{\Sigma}'\hat{\Sigma} \begin{bmatrix} \Sigma'' & \Sigma'' & 0 \\ \Sigma' & \Sigma' & 0 \\ \Sigma & \Sigma & 0 \end{bmatrix} (-)^{2\Sigma} \begin{bmatrix} \Sigma & 0 & \Sigma \\ \Sigma & \Sigma & 0 \\ 0 & \Sigma & \Sigma \end{bmatrix} \left[W^{[\Sigma'']} W^{[\Sigma']} W^{[\Sigma]}\right]^{[0]} \left[Q^{[\Sigma'']} Q^{[\Sigma']} Q^{[\Sigma]}\right]^{[0]}$$

$$
\begin{aligned}
&= \hat{\Sigma}''\hat{\Sigma}'\hat{\Sigma}\frac{\hat{\Sigma}}{\hat{\Sigma}''\hat{\Sigma}'}(-)^{2\Sigma}\frac{(-)^{2\Sigma}}{\hat{\Sigma}\hat{\Sigma}}\left[\left[\tilde{W}^{[\Sigma'']}W^{[\Sigma']}\right]^{[\Sigma]}W^{[\Sigma]}\right]^{[0]}\left[Q^{[\Sigma'']}Q^{[\Sigma']}Q^{[\Sigma]}\right]^{[0]} \\
&= \left[\left[\tilde{W}^{[\Sigma'']}W^{[\Sigma']}\right]^{[\Sigma]}W^{[\Sigma]}\right]^{[0]}\left[Q^{[\Sigma'']}Q^{[\Sigma']}Q^{[\Sigma]}\right]^{[0]} \qquad (39)
\end{aligned}
$$

The invariant weight tensor matrix element may be evaluated for the following particular values of the weight tensors $\left(W_{\sigma''}^{[\Sigma'']}\right)^{\dagger} = (-)^{\Sigma''+\sigma''}\alpha_{\Sigma''}\delta_{-\sigma'',m_{\Sigma''}}$, $W_{\sigma'}^{[\Sigma']} = \alpha_{\Sigma'}\delta_{\sigma',m_{\Sigma'}}$ and $W_{\sigma}^{[\Sigma]} = \alpha_{\Sigma}\delta_{\sigma,m_{\Sigma}}$ where the factor $\alpha_k : k \in \{\Sigma'', \Sigma', \Sigma\}$ is a free phase with unit norm. For this problem, a useful choice is $\alpha_k = (-)^k$. One finds

$$
\begin{aligned}
&\left[\left[\tilde{W}^{[\Sigma'']}W^{[\Sigma']}\right]^{[\Sigma]}W^{[\Sigma]}\right]^{[0]} = \sum_{m_{\Sigma''},m_{\Sigma'},m_{\Sigma}}(-)^{\Sigma''+\sigma''}\times \\
&\qquad (\Sigma''\,\Sigma'\,m_{\Sigma''}\,m_{\Sigma'}|\,\Sigma\,-m_{\Sigma})(\Sigma\,\Sigma\,-m_{\Sigma}\,m_{\Sigma}|\,0\,0)\delta_{-\sigma'',m_{\Sigma''}}\delta_{\sigma',m_{\Sigma'}}\delta_{\sigma,m_{\Sigma}}(-)^{\Sigma''+\Sigma'+\Sigma} \\
&= (-)^{\Sigma''+\sigma''}(-)^{\Sigma''-\Sigma'-\sigma}\hat{\Sigma}\begin{pmatrix}\Sigma'' & \Sigma' & \Sigma \\ -\sigma'' & \sigma' & \sigma\end{pmatrix}\frac{(-)^{\Sigma+\sigma}}{\hat{\Sigma}}(-)^{\Sigma''+\Sigma'+\Sigma} \\
&= (-)^{\Sigma''+\sigma''}(-)^{\Sigma''-\Sigma'+\Sigma}\begin{pmatrix}\Sigma'' & \Sigma' & \Sigma \\ -\sigma'' & \sigma' & \sigma\end{pmatrix}(-)^{\Sigma''+\Sigma'+\Sigma} \qquad (40)
\end{aligned}
$$

Equation 40 gives the invariant weight matrix element. Although the phase can be simplified further, it is useful to leave it in this form as it facilitates subsequent manipulations. For the case of definite operator amplitudes, the result is seen to be proportional to a Wigner 3j symbol with a phase that results from the particular phase convention employed here. The reduced matrix element term $\left[\tilde{Q}^{[\Sigma'']}Q^{[\Sigma']}Q^{[\Sigma]}\right]^{[0]}$ has an additional phase that allows one to express the trace equation in the standard form for the Wigner-Eckart theorem, as will be seen.

In order to evaluate the remaining invariant $\left[\left[\tilde{Q}^{[\Sigma'']}Q^{[\Sigma']}\right]^{[\Sigma]}Q^{[\Sigma]}\right]^{[0]}$, recall that the Q operators are constructed from spin operators S in the form $Q \propto |S, m_s\rangle\langle S, m_s'|$, a product of a tensor that transforms as a ket and one that transforms as a bra, in that order. Figure 6 shows how one may evaluate the reduced matrix element in term of invariants that have already been computed. Some new notation is introduced that simplifies the presentation in more complicated systems. The new notation in Figure 6 is the reduction of two lines to one, *e.g.*, the coupling of two S tensors to a Σ tensor. This feature demonstrates the inheritance structure of the Q spin operators. It will be very useful in constructing an OOP-based approach to the construction of the spin Hamiltonian.

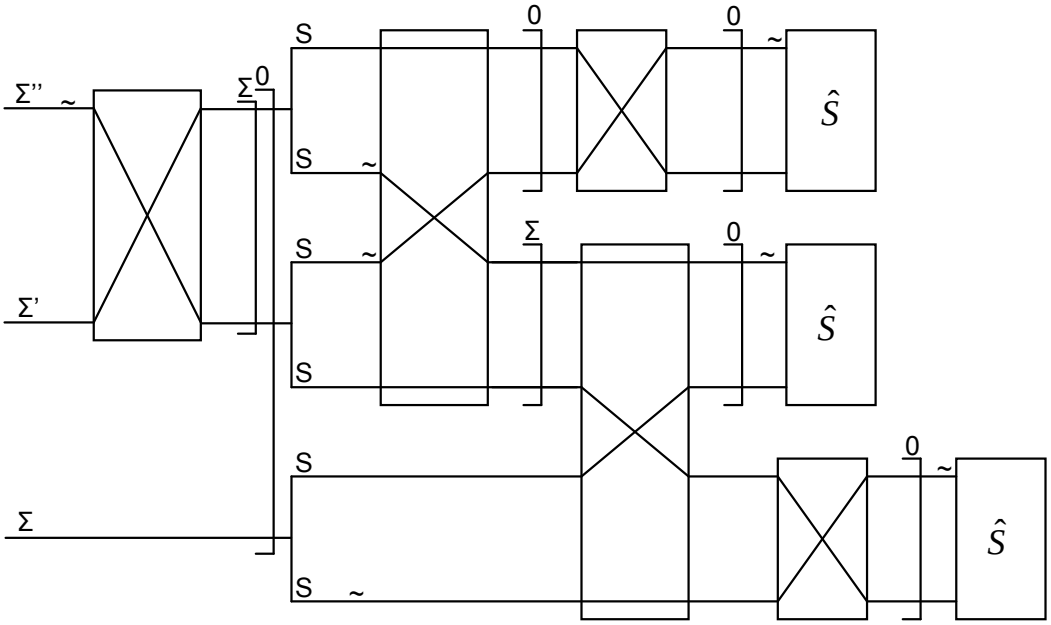

Figure 6: This figure shows the invariant diagram for the reduced matrix element of three Q tensors. It is the final piece in the graphical statement of the Wigner-Eckart theorem. The terminal boxes are invariants that have already been evaluated. See the text for more details.

The analytical form of the invariant graph in Figure 6 is given as follows

$$\left[\left[\tilde{Q}^{[\Sigma'']}Q^{[\Sigma']}\right]^{[\Sigma]}Q^{[\Sigma]}\right]^{[0]} =$$

$$(-)^{\Sigma''+\Sigma'-\Sigma}(-i)^{\Sigma''+\Sigma'+\Sigma}(-)^{\Sigma''}\begin{bmatrix} S & S & \Sigma' \\ S & S & \Sigma'' \\ 0 & \Sigma & \Sigma \end{bmatrix}(-)^{2S}\hat{S}\begin{bmatrix} S & S & \Sigma \\ S & S & \Sigma \\ 0 & 0 & 0 \end{bmatrix}\hat{S}(-)^{2S}\hat{S}$$

$$= (-)^{\Sigma''+\Sigma'-\Sigma}(-i)^{\Sigma''+\Sigma'+\Sigma}(-)^{\Sigma''}(-)^{2S+\Sigma''+\Sigma}\frac{\hat{\Sigma}''\hat{\Sigma}'}{\hat{S}}(-)^{2S-\Sigma}\frac{\hat{\Sigma}}{\hat{S}\hat{S}}(-)^{2S-\Sigma}\hat{S}\hat{S}\hat{S}\begin{Bmatrix} S & S & \Sigma \\ \Sigma' & \Sigma'' & S \end{Bmatrix}$$

$$= (-)^{\Sigma''+\Sigma'-\Sigma}(-)^{2S+\Sigma''+\Sigma'+\Sigma}(-i)^{\Sigma''+\Sigma'+\Sigma}\hat{\Sigma}''\hat{\Sigma}'\hat{\Sigma}\begin{Bmatrix} \Sigma'' & \Sigma' & \Sigma \\ S & S & S \end{Bmatrix}, \tag{41}$$

using the symmetries of the Wigner 6j symbol under interchange of row entries in two columns and

interchange of columns. Equation 41 completes the invariant graph representation of the generalized Wigner-Eckart Theorem. Combining Equations 40 and 41 gives the trace of the product of three Q operators with no additional phase factors. One finds

$$Tr\left\{\left(Q_{\sigma''}^{[\Sigma'']}\right)^{\dagger} Q_{\sigma'}^{[\Sigma']} Q_{\sigma}^{[\Sigma]}\right\} =$$

$$(-)^{\Sigma''-\sigma''}\begin{pmatrix} \Sigma'' & \Sigma' & \Sigma \\ -\sigma'' & \sigma' & \sigma \end{pmatrix}(-)^{\Sigma''+\Sigma'+\Sigma+2S}(i)^{\Sigma''+\Sigma'+\Sigma}\hat{\Sigma}''\hat{\Sigma}'\hat{\Sigma}\begin{Bmatrix} \Sigma'' & \Sigma' & \Sigma \\ S & S & S \end{Bmatrix} \tag{42}$$

$$\equiv (-)^{\Sigma''-\sigma''}\begin{pmatrix} \Sigma'' & \Sigma' & \Sigma \\ -\sigma'' & \sigma' & \sigma \end{pmatrix}\langle \Sigma'' \parallel \Sigma' \parallel \Sigma\rangle \tag{43}$$

where $\langle \Sigma'' \parallel \Sigma' \parallel \Sigma\rangle$ is a reduced matrix element. In order to simplify the phase, and put it in the usual form of the Wigner-Eckart theorem, the observation that $2S + \Sigma''$ must be an integer on account of the 3j symbol triangle relation, which implies that $2\Sigma''$ must be an even integer, and the observation that $2(\Sigma'' - \sigma'')$ is an even integer have been used.

Note that the phase factor $(-i)^{\Sigma''+\Sigma'+\Sigma}$ in Equation 41 expresses the requirement that the Q operators transform as contrastandard kets and that $\left(Q_{\sigma}^{[\Sigma]}\right)^{\dagger} = (-)^{\Sigma+\sigma}Q_{-\sigma}^{[\Sigma]}$. In order to form the trace of a Q operator with a commutator of Q operators one can interchange Σ' and Σ in Equation 42. This requires an odd permutation of the columns of the Wigner 3j symbol which will introduce a phase $(-)^{\Sigma''+\Sigma'+\Sigma}$ and a permutation of two columns of the Wigner 6j symbol which leaves the Wigner 6j symbol unchanged. Performing these operations, one finds

$$Tr\left\{\left(Q_{\sigma''}^{[\Sigma'']}\right)^{\dagger}\left[Q_{\sigma'}^{[\Sigma']}, Q_{\sigma}^{[\Sigma]}\right]\right\} =$$

$$(-)^{\Sigma''-\sigma''}\hat{\Sigma}''\hat{\Sigma}'\hat{\Sigma}\begin{pmatrix} \Sigma'' & \Sigma' & \Sigma \\ -\sigma'' & \sigma' & \sigma \end{pmatrix}\begin{Bmatrix} \Sigma'' & \Sigma' & \Sigma \\ S & S & S \end{Bmatrix}$$

$$\left(1-(-)^{\Sigma''+\Sigma'+\Sigma}\right)(-)^{\Sigma''+\Sigma'+\Sigma+2S}(i)^{\Sigma''+\Sigma'+\Sigma} \tag{44}$$

Equation 44 exactly reproduces Sanctuary and co-workers' result.[6]

4.1 Two Coupled Spins

Using the Q operators defined above, one may construct invariant Q operators of higher order representing pairwise couplings of other Q operators. If $Q^{[\Sigma]}$ is coupled to $Q^{[\Xi]}$ to form $Q^{[\Lambda]}$ one

may write

$$Q_{\lambda}^{[\Lambda]} = \sum_{\sigma,\xi} (\Sigma\, \Xi\, \sigma\, \xi |\, \Lambda\, \lambda) Q_{\sigma}^{[\Sigma]} Q_{\xi}^{[\Xi]}, \tag{45}$$

which automatically satisfies the phase convention established here as one may show from the symmetry properties of the Clebsch-Gordan coefficients. This has the extremely important consequence that no further phase factors or weight factors need to be introduced in order to achieve consistent results. This demonstrates the advantage of working exclusively with properly phased contrastandard tensors.

Figure 7 shows the graph corresponding to the invariant coupling of two Q operators to form a coupled Q operator. This type of graph can occur when a set of $Q^{[\Sigma]}$ operators are constructed from an S spin and a set of $Q^{[\Xi]}$ operators are constructed from an I spin. The hyperfine interaction, for example, can mix the I and S spins and one may represent this by considering the coupling of the $Q^{[\Sigma]}$ and $Q^{[\Xi]}$ operators to form a set of $Q^{[\Lambda]}$ operators. The spin-orbit interaction, where needed, may be handled in an exactly analogous way. The analytical expression corresponding to the graph in Figure 7 is

$$\begin{bmatrix} \Sigma'' & \Xi'' & \Lambda'' \\ \Sigma' & \Xi' & \Lambda' \\ \Sigma & \Xi & \Lambda \end{bmatrix} (-)^{\Xi+\Sigma-\Lambda} \begin{bmatrix} \Sigma & 0 & \Sigma \\ \Sigma & \Xi & \Lambda \\ 0 & \Xi & \Xi \end{bmatrix} =$$

$$\hat{\Lambda}''\hat{\Lambda}'\hat{\Sigma}\hat{\Xi} \begin{Bmatrix} \Sigma'' & \Xi'' & \Lambda'' \\ \Sigma' & \Xi' & \Lambda' \\ \Sigma & \Xi & \Lambda \end{Bmatrix} (-)^{\Xi+\Sigma-\Lambda} \frac{\hat{\Lambda}}{\hat{\Sigma}\hat{\Xi}} (-)^{\Xi+\Sigma-\Lambda}$$

$$= \hat{\Lambda}''\hat{\Lambda}'\hat{\Lambda} \begin{Bmatrix} \Sigma'' & \Xi'' & \Lambda'' \\ \Sigma' & \Xi' & \Lambda' \\ \Sigma & \Xi & \Lambda \end{Bmatrix} \tag{46}$$

The Wigner 9J symbol can be rewritten in a columnar order reflecting the ordering of the operators in the trace of the product of three Λ operators as follows

$$\begin{Bmatrix} \Sigma'' & \Xi'' & \Lambda'' \\ \Sigma' & \Xi' & \Lambda' \\ \Sigma & \Xi & \Lambda \end{Bmatrix} = \begin{Bmatrix} \Lambda'' & \Lambda' & \Lambda \\ \Sigma'' & \Sigma' & \Sigma \\ \Xi'' & \Xi' & \Xi \end{Bmatrix} \tag{47}$$

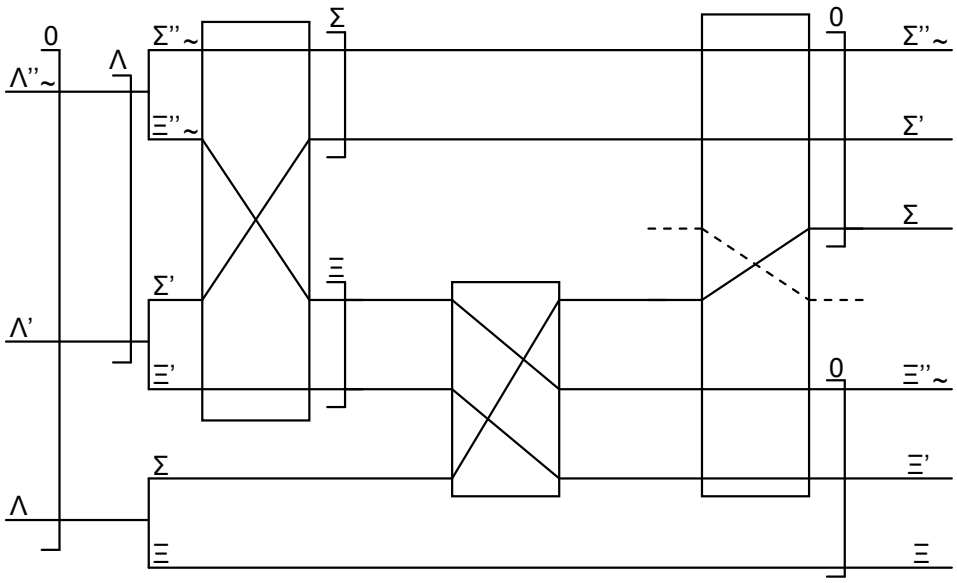

Figure 7: This figure shows the invariant diagram arising from the intermediate couplings of three Q tensors. The analytical form of this graph, given in Equation 46 may be used to resolve intermediate couplings into their final representation in terms of individual spins. The reduced matrix element may then be computed from products of the analytical form of Figure 6. See the text for more details.

using the symmetries of the Wigner 9J symbol.[13] The matrix elements of the spin part of the Hamiltonian superoperator for two coupled spins may therefore be written symbolically as follows

$$
\begin{aligned}
& Tr\left\{\left(Q_{\lambda''}^{[\Lambda'']}\right)^{\dagger}\left[Q_{\lambda'}^{[\Lambda']},Q_{\lambda}^{[\Lambda]}\right]\right\} = \\
& = \left[(-)^{\Lambda''+\lambda''}(-)^{\Lambda''-\Lambda'+\Lambda}\begin{pmatrix}\Lambda'' & \Lambda' & \Lambda\\ -\lambda'' & \lambda' & \lambda\end{pmatrix}\right]\left[\hat{\Lambda}''\hat{\Lambda}'\hat{\Lambda}\begin{Bmatrix}\Lambda'' & \Lambda' & \Lambda\\ \Sigma'' & \Sigma' & \Sigma\\ \Xi'' & \Xi' & \Xi\end{Bmatrix}\right] \\
& \left[(-)^{2S}(i)^{\Sigma''+\Sigma'+\Sigma}\hat{\Sigma}''\hat{\Sigma}'\hat{\Sigma}\begin{Bmatrix}\Sigma'' & \Sigma' & \Sigma\\ S & S & S\end{Bmatrix}\right]\left[(-)^{2I}(i)^{\Xi''+\Xi'+\Xi}\hat{\Xi}''\hat{\Xi}'\hat{\Xi}\begin{Bmatrix}\Xi'' & \Xi' & \Xi\\ I & I & I\end{Bmatrix}\right]
\end{aligned}
$$

$$\left[1-(-)^{\Lambda''+\Lambda'+\Lambda}(-)^{\Lambda''+\Lambda'+\Lambda+\Sigma''+\Sigma'+\Sigma+\Xi''+\Xi'+\Xi}\right] \tag{48}$$

where the first term in square brackets is the contribution from the invariant formed from the weight tensor shown in Figure 5 and evaluated in Equation 40. The second term in square brackets indicates the internal couplings of the invariant Q operator reduced matrix element shown in Figure 5. The internal couplings are shown in Figure 7 and have the analytical form given in Equation 46. The terminating Σ and Ξ couplings, corresponding to the third and fourth square bracket terms originate from two subgraphs of the form given in Figure 6, whose analytical form is given in Equation 41. The phase of the reduced matrix elements incorporates the α_k phase factors introduced in the weight tensor. The phase has been further simplified by noting that in this application $\{\Lambda\}$, $\{\Sigma\}$, $\{\Xi\}$ and all azimuthal quantum numbers are integers so that changing, *e.g.*, $\lambda'' \rightarrow -\lambda''$ does not affect the phase.

The final term in square brackets is the phase difference between terms of the commutator. it arises from the symmetries of the 3j and 9j symbols under permutation of adjacent columns. The 6j symbol is invariant under interchange of any two columns. The phase may be simplified by noting that $\Lambda''+\Lambda'+\Lambda$ must be an integer, thus $2(\Lambda''+\Lambda'+\Lambda)$ must be an even integer, which does not affect the phase. The remaining contributions to the phase yield the simple selection rule that the internal coupling angular momentum values must sum to an odd integer in order for the trace to be non-vanishing. Equation 48 may be further simplified using these observations and rewritten to further emphasize the modular character of the various contributions. One finds

$$\begin{aligned} &Tr\left\{\left(Q_{\lambda''}^{[\Lambda'']}\right)^{\dagger}\left[Q_{\lambda'}^{[\Lambda']},Q_{\lambda}^{[\Lambda]}\right]\right\} = \\ &= \left[(-)^{\Lambda''-\lambda''}\begin{pmatrix}\Lambda'' & \Lambda' & \Lambda\\ -\lambda'' & \lambda' & \lambda\end{pmatrix}(-)^{\Lambda''+\Lambda'+\Lambda}\phi(\{\Sigma\},\{\Xi\})\right]\left[\hat{\Lambda''}\hat{\Lambda'}\hat{\Lambda}\begin{Bmatrix}\Sigma'' & \Xi'' & \Lambda''\\ \Sigma' & \Xi' & \Lambda'\\ \Sigma & \Xi & \Lambda\end{Bmatrix}\right] \\ &\left[(-)^{2S}(i)^{\Sigma''+\Sigma'+\Sigma}\hat{\Sigma''}\hat{\Sigma'}\hat{\Sigma}\begin{Bmatrix}\Sigma'' & \Sigma' & \Sigma\\ S & S & S\end{Bmatrix}\right]\left[(-)^{2I}(i)^{\Xi''+\Xi'+\Xi}\hat{\Xi''}\hat{\Xi'}\hat{\Xi}\begin{Bmatrix}\Xi'' & \Xi' & \Xi\\ I & I & I\end{Bmatrix}\right] \end{aligned} \tag{49}$$

where $\phi(\{\Sigma\},\{\Xi\}) = \left[1-(-)^{\Sigma''+\Sigma'+\Sigma+\Xi''+\Xi'+\Xi}\right]$ is the factor that results from the commutator.

Written in this form, Equation 49 exactly reproduces Sanctuary's results.[6] In order to represent

Equation 49 graphically, it is not necessary to indicate all of the details of the internal recouplings as they have already been evaluated separately in modular fashion, as shown above. Thus, one may express the spin part of matrix elements of the Hamiltonian superoperator in a more abstract graphical form, as shown in Figure 8. Equation 49 expressed in this form is also a suitable starting point for a GUI-based coupled spin Hamiltonian tool. Note that each line leading to an operator

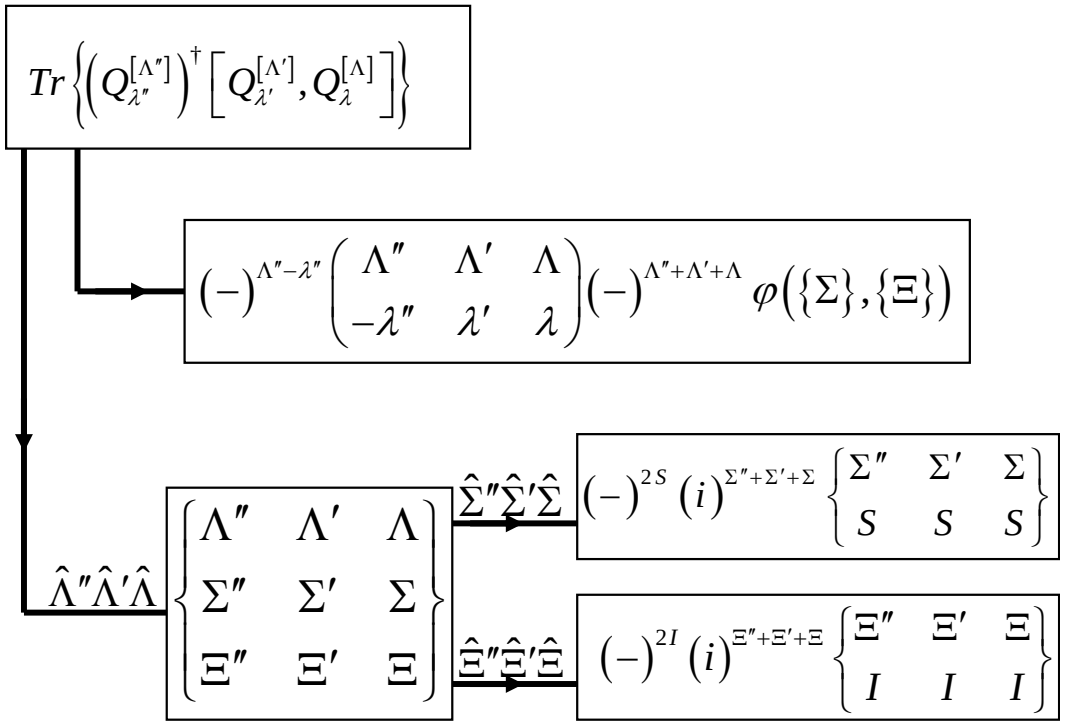

Figure 8: This figure shows a more abstract representation of the recouplings in Equation 49. It is unnecessary to show the details of the intermediate internal couplings, as they have already been worked out by other means. See the text for more details.

invariant in Figure 8 is multiplied by a product of three weights corresponding to the angular momenta values that are recoupled at the input of subsequent boxes. Each box has a phase and amplitude derived earlier. The analytical expression for the initial box is the product of the weight of each line and the contents of the recoupling boxes. Note that for the problems considered so far, the weight box proportional to a 3j symbol is the invariant representation of a projection operator. The formalism can also handle linear combinations of weight tensor components as will be shown

subsequently. This procedure is useful for constructing K symmetrized matrix elements and basis sets, for example, or, equivalently, incorporating crystallographic symmetries into the description.

4.2 Four Coupled Spins

Distance determinations in spin-labeled macromolecules can yield important insights into structure, which in turn inform models of function. Due to the large magnetic moments of nitroxide spin labels, distance measurements *via* double quantum coherence (DQC) EPR can probe intramolecular distances from 1 to 8 nm.[26] When DQC is infeasible, distance determinations may still be made using alternative experimental techniques such as DEER or PELDOR.[27] When nitroxide spin labels are used, dipolar coupling of the two relevant electrons in addition to the coupling of the nitrogen nuclei to the individual electrons (and in principle to each other), yields a system of four coupled spins. The multipole operator method is particularly useful for this case. The appropriate generalization of the Q operator to this case is

$$Q_{\kappa_i}^{[K_i]} = \sum_{\lambda_i,\lambda_i'} (\Lambda_i\, \Lambda_i'\, \lambda_i\, \lambda_i' |\, K_i\, \kappa_i) Q_{\lambda_i}^{[\Lambda_i]} Q_{\lambda_i}^{[\Lambda_i]}, \tag{50}$$

which is of the same form as Equation 45. This important result is the key to treating systems of many coupled spins, as it indicates that successive pairwise couplings of intermediate angular momenta will contribute a factor of the form of Equation 46. A graphical representation of the matrix elements in transition or Liouville space of three $Q_\kappa^{[K]}$ operators can readily be written down by analogy with Figure 8. Figure 9 is one possible realization of this idea. In order to simplify the presentation somewhat, the convention is introduced that a line with an arrow has a weight given by the invariant amplitudes of the arguments of the row or the box in which the arrow terminates. For example, the arrow terminating in the row containing three K arguments in Figure 9 has a weight $\hat{K}_1\hat{K}_2\hat{K}_3$. Boxes containing 9 arguments represent a 9j symbol. The terminating boxes are reduced matrix elements, *e.g.*,

$$\langle \Sigma'' S \parallel \Sigma' \parallel \Sigma S \rangle = (-)^{2S} (i)^{\Sigma''+\Sigma'+\Sigma} \begin{Bmatrix} \Sigma'' & \Sigma' & \Sigma \\ S & S & S \end{Bmatrix}. \tag{51}$$

The commutator phase factor may be written as $1-(-)^{\varphi}$ where φ is the sum of all arguments in Figure 9 connected by directed lines, with the exception of the top level K couplings. The

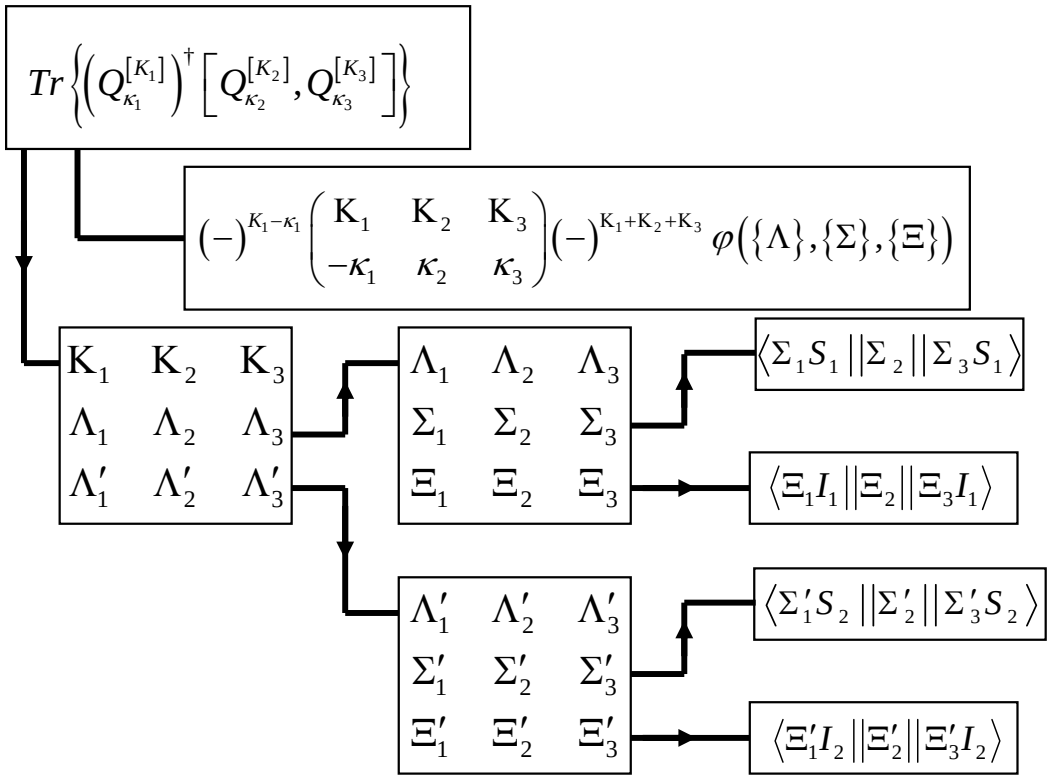

Figure 9: This figure shows an abstract representation of the matrix elements of four coupled spins. Its analytical expression is equivalent to the results of Sanctuary and coworkers.[6] See the text for more details.

analytical representation of Figure 9 exactly reproduces Sanctuary's results. [6]

5 Comparison of Graphical and Algebraic Techniques

In order to have a clear understanding of the commonalities and differences between the graphical techniques of Jucys[10, 11] and Danos[12, 18] on the one hand, and algebraic techniques on the other, it is useful to have a representation of equivalent expressions in the various formalisms, as shown in Figure 10. Here, the subdiagram in the upper left corner is a Jucys nodal diagram expressed in terms of Clebsch-Gordan coefficients, which requires that the node be decorated with a triangle.[11] This is equivalent to a description in terms of Wigner 3j coefficients. As an example of the latter, Appendix B gives a derivation of Equation 8 where the Wigner 9j symbol is expressed

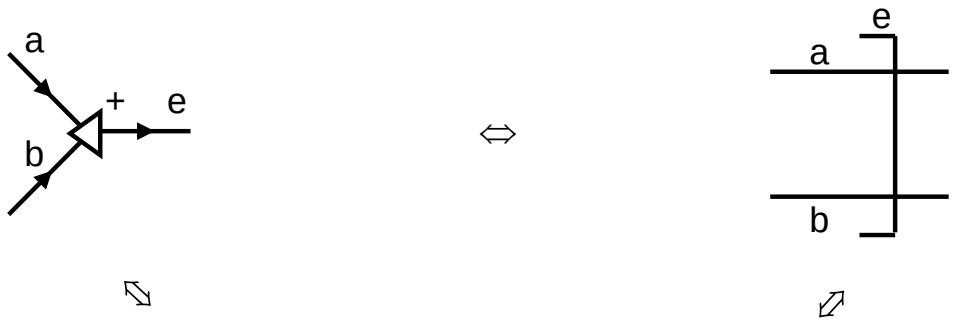

$$\sum_{m_a, m_b} \left(a \quad m_a \quad b \quad m_b \,|\, e \quad m_e\right) \left|a \quad m_a\right\rangle \left|b \quad m_b\right\rangle$$

Figure 10: Diagrammatic and algebraic representations of the coupling of two states to form a third. Starting from the upper left corner and progressing clockwise, one has the Jucys nodal diagram expressed in terms of Clebsch-Gordan coefficients, a pair of coupled Danos lines and the analytical expression in terms of Clebsch-Gordan coefficients.

in terms of Wigner 3j symbols. For those calculations, the nodes are decorated with solid circles. The utility of the distinction between the two kinds of nodes is discussed thoroughly in El Baz and Castel.[11] The diagram shown in the upper right corner of Figure 10 is the Danos representation of the same coupling. Note the absence of arrows and node orientations. This is possible because Danos' notation always expresses coupled tensor quantities in terms of contrastandard tensors, with a 'standard' orientation equivalent to the Jucys node notation. The analytical expression is equivalent to both of the graphical expressions and gives the standard coupling explicitly in terms of Clebsch-Gordan coefficients.

Recoupling of coupled tensor quantities has been constantly employed in this work to simplify traces over products of spin multipole operators. At this point it is useful to examine more carefully how the rules for manipulating these quantities are established. In order to do, the steps in transforming the Jucys nodal diagram for the recoupling of spins $a, b \rightarrow e$ and $c, d \rightarrow f$ to $a, c \rightarrow g$

and $b, d \rightarrow h$ are shown in Figure 11. For the reader for whom the manipulations of Jucys diagrams

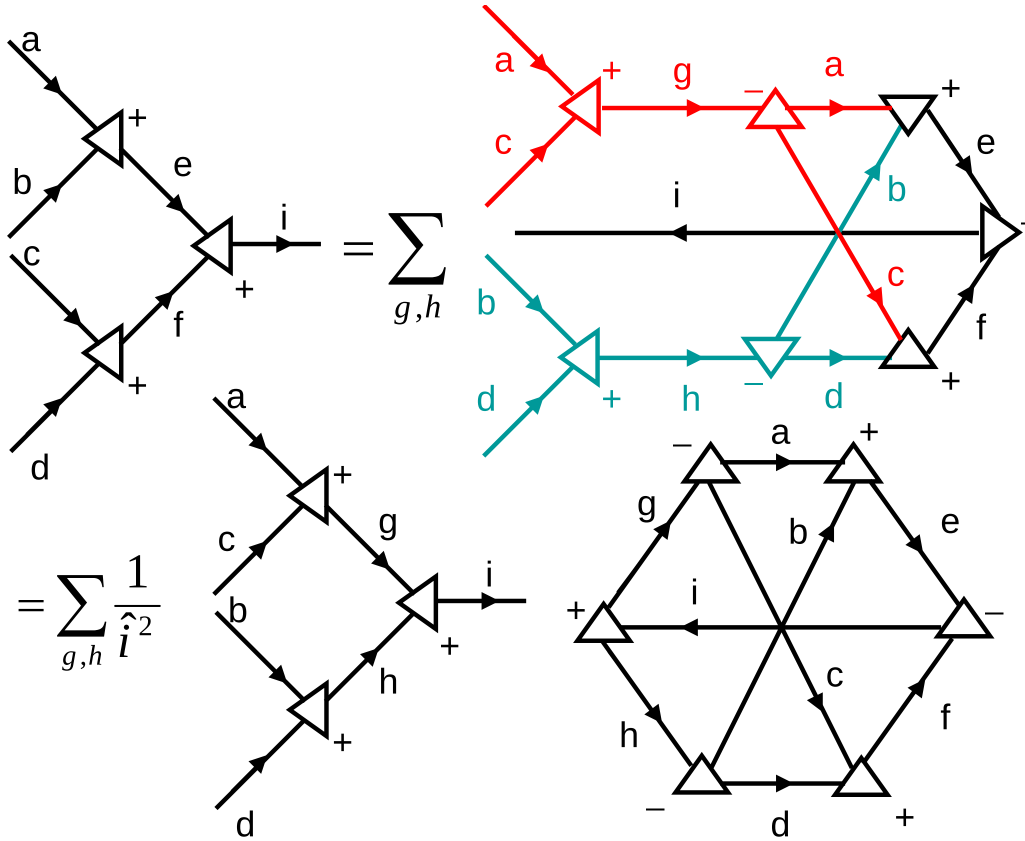

Figure 11: Diagrammatic representations of the coupling of four states to form a tensor object of rank i. The nodal ordering and line orientations are chosen to obey the Danos convention, so that contrastandard tensor quantities may always be used. The red and sea green lines indicate the insertion of unit matrices as discussed in the appendices.

is unfamiliar, Appendix B provides a brief overview of Jucys diagrammatic techniques. The nodal layout is chosen to enforce the contrastandard convention of Danos. The transformations of the diagram correspond to the insertion of factors of unity or scaled identity operators. This class of diagram occurs in the transformation of JJ to LS coupling, for example. The final hexagonal object with no outgoing or incoming lines is the vector coupling coefficient for four angular momenta. It is proportional to a Wigner 9j symbol. It is equivalent, up to normalization factors, to the Wigner 9j symbol derived in Appendix B.

Note that the sum in Figure 11 decomposes into the product of two terms: the first term is the

recoupled tensor of rank i; the second term is the recoupling matrix summed over the 'internal' angular momenta g and h. This is a feature of angular momentum recoupling: the recoupled state will often have a sum over 'intermediate' angular momenta. An example of this occurred in the derivation of Equation 8. For other recoupling problems treated here, there was no sum over 'intermediate' angular momenta, because constraints imposed by the final couplings forced the sums over 'intermediate' angular momenta to degenerate to a single term.

Figure 11 contains the clue for understanding the very different nature of Danos' diagrammatic techniques vis-à-vis those of Jucys. The objects with 'open' lines in Figure 11 indicating the initial or final recouplings are treated as part of a *transformed* object in Jucys' approach. That is to say, in Jucys', diagrammatic approach, the transformations are all done 'in place'. In Danos' approach, on the other hand, recouplings are treated as a *progressive* mutation of the initial tensor couplings. These considerations are represented graphically in Figure 12. It is the progressive nature of Danos' representation that allows the recouplings to be expressed in terms of a flowchart or circuit schematic. From the circuit perspective, the tensor recouplings may be thought of as filter functions which modify the signal traveling down a transmission line. Here the Wigner 9j symbols plays the role of the transfer function. Using the insights gleaned from this exercise, it is now clear why the recoupling box representation of Danos, first introduced in Figure 1, has the form it does. The recoupling rule which requires summation over 'intermediate' angular momenta is now easily understood as well.

This is a very different perspective on the recoupling problem. It is precisely this alternative perspective that allows one to follow the 'history' of the recoupling transformations in diagrammatic form at a glance. As one has direct access to the sequence of transformations in Danos' approach, vis-à-vis Jucys' approach, one may exploit more easily the modularity of multiple spin recouplings. This consideration is very important for the GUI-based approach to constructing the Hamiltonian discussed below.

It is important to note that this author views the approaches of Jucys and Danos to be complementary. The Jucys approach is more flexible, in that it can handle costandard and contrastandard tensor quantities, in addition to problems where multiple spins are coupled directly. In such problems, where 12j, 15j, ..., and so on occur, the methods of Jucys are superior to those of Danos.

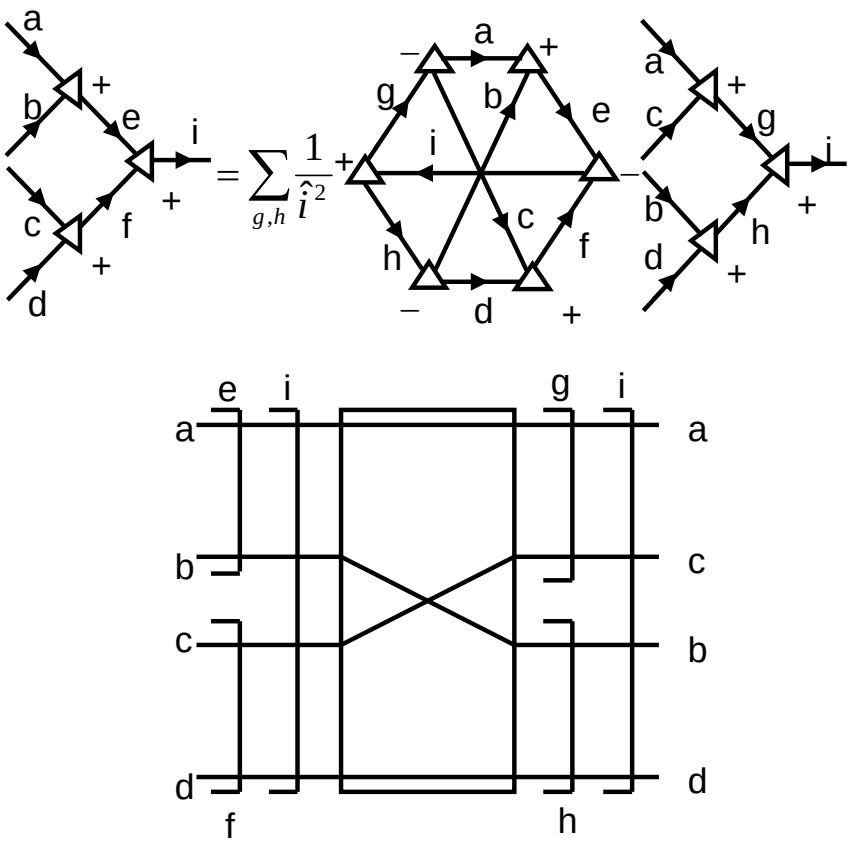

Figure 12: Jucys and Danos representations of the recoupling of four tensors forming a tensor of rank i. In the Jucys approach, transformations are all done 'in place'. In the Danos approach, transformations are sequential.

However, in most practical problems in atomic, molecular and magnetic resonance spectroscopy, spins are coupled pair-wise and one need only consider Wigner 6j and 9j symbols. For such cases, the methodology of Danos has definite advantages. In this author's estimation, those advantages consist of the following: *progressive* transformation of tensor recouplings, which allows a *modular* approach to solving recoupling problems; a *consistent* phase convention that allows one to *dispense* with oriented nodes and directed lines.

In order to make the connection to algebraic methods explicit, the analytic representation of

the the recoupling box in terms of vector coupling coefficients is

$$| \, (ab)_e \, (cd)_f \, ; i \, m_i \, \rangle \;\; = \;\; \sum_{g,h} \hat{e} \hat{f} \hat{g} \hat{h} \left\{ \begin{array}{ccc} a & b & e \\ c & d & f \\ g & h & i \end{array} \right\} | \, (ac)_g \, (bd)_h \, ; i \, m_i \, \rangle \tag{52}$$

$$= \;\; \sum_{g,h} \langle \, (ab)_e \, (cd)_f \, i \, | \, (ac)_g \, (bd)_h \, i \, \rangle | \, (ac)_g \, (bd)_h \, ; i \, m_i \, \rangle \tag{53}$$

While there are important differences between the diagrammatic techniques of Danos and Jucys, it is also important to note that there are points of similarity as well. Sometimes, the connections are not obvious. If one compares the diagrammatic proofs of Equation 8 given in Figure 2 and Figure 15 it is difficult to read off the connections among the various steps, given the correspondence $a \leftrightarrow j_1$, $b \leftrightarrow j_2$, $e \leftrightarrow j_3$, $c \leftrightarrow l_1$, $d \leftrightarrow l_2$, $f \leftrightarrow l_3$, $g \leftrightarrow k_1$, $h \leftrightarrow k_2$, $i \leftrightarrow k_3$. If one interchanges the first two columns and rows of the vector coupling coefficient, which does not affect its phase or amplitude, and relabels the momenta as appropriate, the recoupling scheme in Figure 2 and Figure 15 are in one to one correspondence. This is an example of the flexibility of angular momentum recouplings; there are many equivalent representations of Equation 8. The graphical proof shown in Figure 2 represents Biedenharn and Louck's symbolic expression. Figure 15 is patterned on the equivalent but differently realized graphical proof in El Baz and Castel. The different representations were chosen to facilitate comparison of the Danos diagrammatic technique with the original derivations by other means. Some explicit identifications may clarify matters. The equivalence between the Danos and Jucys approaches may be written in terms of the four angular momentum vector coupling coefficients as follows

$$\left[\begin{array}{ccc} a & b & e \\ c & d & f \\ g & h & i \end{array} \right] = \sum_{l} \left[\begin{array}{ccc} a & b & e \\ 0 & f & f \\ a & l & i \end{array} \right] \left[\begin{array}{ccc} 0 & b & b \\ c & d & f \\ c & h & l \end{array} \right] \left[\begin{array}{ccc} a & 0 & a \\ c & h & l \\ g & h & i \end{array} \right] \tag{54}$$

The first point to emphasize is that a vector coupling box with one zero is proportional to a Wigner 6j symbol. The second point is that the insertion of the angular momentum line l and the separation over three angular momentum lines discussed in Appendix B may also be read off of Equation 54. In order to facilitate this identification, the author has indicated the rows and columns corresponding to the insertion of the l line in red and the two separations over three

angular momentum lines in blue. Entries that participate in both processes are represented in purple. Reexpressing Equation 54 in terms of Wigner 9j and 6j symbols, one finds

$$\left\{ \begin{array}{ccc} a & b & e \\ c & d & f \\ g & h & i \end{array} \right\} = \sum_{l} \hat{l}^2 (-)^{2l} \left\{ \begin{array}{ccc} a & b & e \\ f & i & l \end{array} \right\} \left\{ \begin{array}{ccc} c & d & f \\ b & l & h \end{array} \right\} \left\{ \begin{array}{ccc} g & h & i \\ l & a & c \end{array} \right\} \tag{55}$$

Note that the unmarked angular momenta, e, d and g are equivalent to the three angular momenta j_3, l_2 and k_1 of Figure 15 that do not participate in the separation over three lines or the insertion of the l (x) angular momentum.

The feature of Danos' graphical technique that is relevant to these observations is that the intermediate angular momentum lines in a Danos diagram correspond to separations over lines in a Jucys diagram. Given that separation over lines for the relevant cases considered generates Wigner 6j or 9j symbols, one sees that the recoupling boxes in a Danos diagram are scalar objects that satisfy the commutation property. Thus, one need not preserve the order of recoupling boxes, as they are numbers (scalars) that commute. In order to keep track of the terms in the analytical expression of a Danos diagram it is conventional to order the factors top to bottom and left to right. This is merely a convenience, however, not a necessity.

6 Matrix Elements of the Hamiltonian Superoperator

In electron paramagnetic resonance (EPR) lineshape calculations, all workers regard the review articles of Schneider and Freed as touchstones.[30, 31] Fortunately, the work reported on here is consistent with the conventions established by Schneider and Freed, as will be seen. These conventions involve important points of Angular Momentum Hygiene, for lack of a better term. Workers in EPR theory who disregard them, do so at their own peril. One point that needs to be clarified immediately is the ISTO basis for representing vector operators. Biedenharn and Louck[3] note that the phase convention for the spherical basis vectors of Danos and Gillet [18] and Sanctuary

[3] *ibid.* pp. 169–179.

[6] may be expressed in the following form

$$\begin{aligned}\hat{\eta}_{+1} &= -\frac{\alpha}{\sqrt{2}}\left(\hat{e}_1 + i\hat{e}_2\right) \\ \hat{\eta}_0 &= -i\hat{e}_3 \\ \hat{\eta}_{-1} &= -\frac{\alpha*}{\sqrt{2}}\left(\hat{e}_1 - i\hat{e}_2\right)\end{aligned} \tag{56}$$

where $\hat{\eta}$ is a spherical basis that has the property that makes $\hat{\eta}\cdot\hat{\eta}$ and $\hat{\eta}\times\hat{\eta}$ real. Here α is a unimodular complex constant. Danos [12] chooses $\alpha = -i$. Sanctuary and coworkers [6] choose $\alpha = i$ which has a relative minus sign to the choice of Danos. Biedenharn and Louck[4] note that the choice is arbitrary. For the current application, the difference between Sanctuary and Danos' convention is the phase factor $\alpha_\Sigma = (-)^\Sigma$ in the weight tensors used in the invariant graph method.

Schneider and Freed define an ISTO with the following behavior under coordinate transformations

$$T_i^{(J,M)} \rightarrow T_f^{(J,M)} = \sum_{M'=-J}^{J} T_i^{(J,M')}\mathcal{D}^J_{M'M}\left(\Omega_{i\rightarrow f}\right) \tag{57}$$

which is the same convention used by Danos and Gillet.[18] The Hamiltonian, which must transform as a scalar (or rank 0 tensor) under coordinate transformations may be written as

$$\begin{aligned}\mathcal{H} &= \sum_{l,m}\hat{l}(l\,l\,-m\,m|\;0\,0)F^{[l]}_{-m}(\Omega)A^{[l]}_m \\ &= \sum_{l,m}\hat{l}\frac{(-)^{l+m}}{\hat{l}}F^{[l]}_{-m}(\Omega)A^{[l]}_m,\end{aligned} \tag{58}$$

where the $\{F\}$ tensors define the weights for the Hamiltonian. Note that the relevant values of l are $l = 0, 2$, thus Equation 58 is equivalent to the phase and amplitude convention (due to the extra factor $\hat{l}$) of Schneider and Freed

$$\mathcal{H} = \sum_{\{l:l=0,2\},m}(-)^m F^{(l,-m)}(\Omega)A^{(l,m)} \tag{59}$$

Some examples may make the notation and correspondence clearer between the two formalisms. The spherical basis

$$\hat{\eta}_{+1} = \frac{i}{\sqrt{2}}\left(\hat{e}_1 + i\hat{e}_2\right)$$

[4] *idem.*

$$\begin{aligned} \hat{\eta}_0 &= -i\hat{e}_3 \\ \hat{\eta}_{-1} &= -\frac{i}{\sqrt{2}}\left(\hat{e}_1 - i\hat{e}_2\right) \end{aligned} \tag{60}$$

implies the following values for the ISTO's corresponding to the electron Zeeman interaction

$$F_0^{[0]}(g_e, \mathrm{mol}) = \left(\frac{\beta_e}{\hbar}\right)\frac{1}{\sqrt{3}}\left(g_{xx} + g_{yy} + g_{zz}\right) \tag{61}$$

$$F_{\pm 2}^{[2]}(g_e, \mathrm{mol}) = -\left(\frac{\beta_e}{\hbar}\right)\frac{1}{2}\left(g_{xx} - g_{yy}\right) \tag{62}$$

$$F_{\pm 1}^{[2]}(g_e, \mathrm{mol}) = 0 \tag{63}$$

$$F_0^{[2]}(g_e, \mathrm{mol}) = -\left(\frac{\beta_e}{\hbar}\right)\sqrt{\frac{2}{3}}\left(g_{zz} - \frac{1}{2}\left(g_{xx} + g_{yy}\right)\right) \tag{64}$$

and the hyperfine interaction

$$F_0^{[0]}(A, \mathrm{mol}) = \left(\frac{g_e\beta_e}{\hbar}\right)\frac{1}{\sqrt{3}}\left(A_{xx} + A_{yy} + A_{zz}\right) \tag{65}$$

$$F_{\pm 2}^{[2]}(A, \mathrm{mol}) = -\left(\frac{g_e\beta_e}{\hbar}\right)\frac{1}{2}\left(A_{xx} - A_{yy}\right) \tag{66}$$

$$F_{\pm 1}^{[2]}(A, \mathrm{mol}) = 0 \tag{67}$$

$$F_0^{[2]}(A, \mathrm{mol}) = -\left(\frac{g_e\beta_e}{\hbar}\right)\sqrt{\frac{2}{3}}\left(A_{zz} - \frac{1}{2}\left(A_{xx} + A_{yy}\right)\right) \tag{68}$$

The relative minus sign between the results given here and those reported by Schneider and Freed are due to the different spherical tensor bases employed. Since rank 0 and rank 2 tensors will always be contracted with rank 0 and rank 2 tensors respectively, the extra phase factor drops out of the formalism.

In order to construct the terms in the Hamiltonian that model the interaction of the applied magnetic field(s), one may use a very general form, based on the convention for the spherical basis adopted here.

$$B_{\pm 1}^{[1]} = \pm\frac{i}{\sqrt{2}}\left(B_x \pm iB_y\right), B_0^{[0]} = -iB_z. \tag{69}$$

This form may be used to represent the effects of time-varying or static fields. It will also be useful for studying the effects of modulation, etc. One may now construct the Zeeman interactions in the coupled basis.

6.1 Zeeman Interactions

For this set of interactions, one may project out specific pieces of the Q operators in order to construct the required Hamiltonian matrix elements.

6.1.1 Two Coupled spins S and I

In general, the S spin is used to construct the Σ operators and the I spins are used to construct the Ξ operators. For the electron Zeeman interaction, one couples only the $\Xi = 0$ operators with the Σ operators. This contribution to the Hamiltonian is therefore in the form

$$\mathcal{H}(g_e) = \sum_l \hat{l} \left[F^{[l]}(g_e, \text{lab}) \left[Q^{[1]}(\Sigma = 1, \Xi = 0) B^{[1]} \right]^{[l]} \right]^{[0]}, \tag{70}$$

where the F tensors play the same role as the weight tensors introduced in Section 3.4, but with a normalization that is no longer dimensionless

$$\begin{aligned} F^{[2]} \odot^2 F^{[2]} &\equiv \left[F^{[2]} F^{[2]} \right]^{[0]} \\ &= \frac{1}{\hat{2}} \left(\frac{\beta_e}{\hbar} \right)^2 \left[\frac{1}{4} \left(g_{xx} - g_{yy} \right)^2 + \frac{2}{3} \left(g_{zz} - \frac{1}{2} \left(g_{xx} + g_{yy} \right) \right) \right]. \end{aligned} \tag{71}$$

The contraction is a frame invariant statement, but in order to have a consistent description, note that the F tensors must be expressed in the lab frame when contracted with the spin multipole operators, which requires coordinate transformations of the sort discussed in the review article of Schneider and Freed.[30] In general, this transformation has a stochastic time-dependence, which is the operative mechanism in spin relaxation. Note also, that $\vec{B} \cdot \vec{B} = \hat{1} \left[B^{[1]} B^{[1]} \right]^{[0]} = B_x^2 + B_y^2 + B_z^2$.

6.1.2 Nuclear Zeeman

The nuclear Zeeman interaction can be significant in EPR time domain experiments[5] and under low field or slow-tumbling conditions[32]. One may use the formalism given here to account for a fully anisotropic chemical shift anisotropy by making the appropriate substitutions in Equation 64, although it should be noted that an isotropic nuclear Zeeman interaction is almost invariably assumed for EPR lineshape calculations. Equation 70 may then be used with $\Sigma = 0$, and $\Xi = 1$.

6.1.3 Four Coupled Spins

In this case, the internal couplings are represented by the labels Σ, corresponding to S_1, Σ', corresponding to S_2, Ξ corresponding to I_1 and Ξ' corresponding to I_2. The Zeeman interactions may be written down, using the appropriate form of Equation 64 and Equation 70, where the electron Zeeman interaction for S_2, say, is selected by choosing $\Sigma = 0$, $\Sigma' = 1$, $\Xi = 0$, $\Xi' = 0$.

6.2 Hyperfine Interaction

The Hyperfine interaction accounts for couplings between an S spin and I spin where $\Sigma = 1$ and $\Xi = 1$.

6.2.1 Two Coupled Spins

In this case, the Hyperfine contribution to the Hamiltonian may be written in the following form

$$\mathcal{H}(\text{hyp}) = \sum_l \hat{l} \left[F^{[l]}(A, \text{lab}) Q^{[l]}(1,1) \right]^{[0]}, \tag{72}$$

where a shorthand notation for $Q^{[l]}(\Sigma, \Xi)$ has been introduced.

6.2.2 Four Coupled Spins

The Q operators for four coupled spins may be disambiguated by specifying the relevant Σ and Ξ labels as follows $Q^{[l]} \rightarrow Q^{[l]}(\Sigma, \Xi, \Sigma', \Xi')$. Thus, the hyperfine coupling between S_1 and I_1 may be written as

$$\mathcal{H}(\text{hyp}_1) = \sum_l \hat{l} \left[F^{[l]}(A_1, \text{lab}) Q^{[l]}(1,1,0,0) \right]^{[0]}, \tag{73}$$

and the hyperfine coupling between S_2 and I_2 has the form

$$\mathcal{H}(\text{hyp}_2) = \sum_l \hat{l} \left[F^{[l]}(A_2, \text{lab}) Q^{[l]}(0,0,1,1) \right]^{[0]}, \tag{74}$$

in an obvious notation. This formalism may be extended in a straightforward way to couplings between, *e.g.*, S_1 and I_2, say, if needed.

6.3 Non-hyperfine Dipole-Dipole Couplings

In this case, one typically has a coupling between S_1 and S_2, for which $\Sigma = \Sigma' = 1$ and $\Xi = \Xi' = 0$. For traceless representations of these couplings, the Hamiltonian takes the following form

$$\mathcal{H}(\text{dip-dip}_S) = \left[F^{[2]}(\text{dip-dip}_S, \text{lab})Q^{[2]}(1,0,1,0)\right]^{[0]}. \tag{75}$$

If needed, nuclear dipole-dipole couplings may be treated in similar fashion. For distance measurements in EPR, it may be useful to use a hybrid coupling scheme where the coupled representation is used for (S_1, I_1) and (S_2, I_2) but dipole-dipole interactions are treated in an uncoupled basis.[6] For electron-electron double resonance (ELDOR) where slow-tumbling can cause strong couplings[32] it may still be advantageous to use the coupled representation.

6.4 Zero Field Splittings, Nuclear Quadrupole and Stevens Operators

For these interactions, Σ and Ξ values larger than 1 are relevant. Such Σ and Ξ values can only occur for systems where $S, I \geq 1$. Given that no restrictions have been placed on allowed values of S and I in the spin multipole formalism, one may use the same code for doublet and triplet EPR. All that is required is the proper specification of the Σ and Ξ values. In a four spin problem, for example, if $S_1 = 1$, the zero field splitting term would be computed from

$$\mathcal{H}(\text{zfs}_1) = \left[F^{[2]}(\text{zfs}_1, \text{lab})Q^{[2]}(2,0,0,0)\right]^{[0]}, \tag{76}$$

where it is assumed that the zero field splitting has been expressed in traceless form. In a similar vein, the nuclear quadrupole contribution for I_2 would be

$$\mathcal{H}(\text{quad}_2) = \left[F^{[2]}(\text{quad}_2, \text{lab})Q^{[2]}(0,0,0,2)\right]^{[0]}. \tag{77}$$

If a given interaction is expressed in terms of Stevens operators, one may use standard tables to convert them to the ISTO's used here.[33]

6.5 General Hamiltonian Superoperator Matrix Elements

With the notation introduced here, the Hamiltonian may be split into Zeeman and non-Zeeman parts

$$\mathcal{H} = {\sum_{\mu,l}}' \hat{l} \left[F^{[l]}(\mu, \text{lab}) Q^{[l]}(\mu; \Sigma, \Xi, \Sigma', \Xi') \right]^{[0]} + \sum_{\nu,l} \hat{l} \left[F^{[l]}(\nu, \text{lab}) \left[Q^{[1]}(\nu; \Sigma, \Xi, \Sigma', \Xi') B^{[1]}(\nu) \right]^{[l]} \right]^{[0]}, \tag{78}$$

where μ labels non-Zeeman interactions and ν labels all possible Zeeman-like terms corresponding to modulaiton fields, multiple resonance, etc. The prime on the μ summation is a reminder that only non-Zeeman terms are included in that summation.

Assembling all of the results derived so far, one may write down the general expression for the matrix elements of the Hamiltonian superoperator as follows

$$\begin{aligned}
&\text{Tr}\left\{ \left(Q^{[\Lambda_1]}_{\lambda_1} \right)^\dagger \mathcal{H}^\times Q^{[\Lambda_3]}_{\lambda_3} \right\} = \\
&\quad {\sum_{\{\mu\},\Lambda_2,\lambda_2}}' (-)^{\Lambda_2+\lambda_2} F^{[\Lambda_2]}_{-\lambda_2}(\mu_2) (-)^{\Lambda_1-\lambda_1} \begin{pmatrix} \Lambda_1 & \Lambda_2 & \Lambda_3 \\ -\lambda_1 & \lambda_2 & \lambda_3 \end{pmatrix} \langle \Lambda_1(\mu_1) \| \, \Lambda_2(\mu_2) \, \| \Lambda_3(\mu_3) \rangle \\
+ &\quad \sum_{\{\nu\},\Lambda_2,\lambda_2,q} (-)^{\Lambda_2+\lambda_2} F^{[\Lambda_2]}_{-\lambda_2}(\nu_2) B^{[1]}_{\lambda_2-q}(\nu_2) (1\, 1\, q\, \lambda_2 - q | \, \Lambda_2\, \lambda_2) \times \\
&\quad \times (-)^{\Lambda_1-\lambda_1} \begin{pmatrix} \Lambda_1 & \Lambda_2 & \Lambda_3 \\ -\lambda_1 & \lambda_2 & \lambda_3 \end{pmatrix} \langle \Lambda_1(\nu_1) \| \, 1(q) \, \| \Lambda_3(\mu_3) \rangle
\end{aligned} \tag{79}$$

where the reduced matrix elements in Equation 79 may be evaluated using the methods of Section 4. The labels μ and ν keep track of which set of Σ and Ξ labels are needed for a particular Hamiltonian superoperator matrix element.

7 Comments on the Generalized Wigner-Eckart Theorem

In a sense, many of the results for multiple coupled spins had already been worked out, once the primitive reduced matrix element in Equation 51 was derived. Consider the two spin problem, where the spin S generate the Σ multipole operators, the spin I generates the Ξ operators and both are coupled to a Λ tensor. The reduced matrix element for a Σ and Ξ operator coupled to a

Λ operator is known to be (*mutatis mutandis*)[8, 9, 11, 13, 21, 23, 34]

$$\langle\, \Lambda''\,(\Sigma'',\Xi'')\, \parallel \Lambda'\,(\Sigma',\Xi')\, \parallel \Lambda\,(\Sigma,\Xi)\,\rangle = \langle\, \Sigma'' S \parallel \Sigma' \parallel \Sigma S\,\rangle\langle\, \Xi'' I \parallel \Xi' \parallel \Xi I\,\rangle \hat{\Lambda}''\hat{\Lambda}'\hat{\Lambda} \left\{ \begin{array}{ccc} \Lambda'' & \Lambda' & \Lambda \\ \Sigma'' & \Sigma' & \Sigma \\ \Xi'' & \Xi' & \Xi \end{array} \right\} \tag{80}$$

Equation 80 may be applied recursively until one is left with products of primitive irreducible matrix elements of the form given in Equation 51. As an exercise, the reader may apply this process to the treatment of four coupled spins given in Section 4.2. This algebraic formulation, which is complementary to the diagrammatic approach discussed in Section 4, is equivalent to the algebraic approach developed in, *e.g.*, Sanctuary, and coworkers.[6] The reader may decide for him- or herself which approach is the most useful in a given application, but from this author's perspective, the diagrammatic approach displays the couplings in the clearest fashion.

Another point to make is that if the spins are always considered to be coupled pair-wise, then the highest 3nj symbol that needs to be considered is the Wigner 9j symbol. Given the couplings that are the most common in magnetic resonance experiments, more complicated couplings, which would require, *e.g.*, Wigner 12j and higher symbols could more easily be modeled in most cases by a phenomenological contribution to the homogeneous or inhomogeneous broadening.

Finally, the Wigner-Eckart theorem assumes an integration over continuous coordinates and a sum over discrete coordinates. This procedure was used to construct the invariants given in Equations 28 and 30. From the perspective of a Danos graph or a Jucys graph, the only 'free' lines are in the initial couplings corresponding to the invariant triple product of three weight tensors, which is proportional to a Wigner 3j symbol as shown in Equation 40. This is the 'geometrical' part of the Wigner-Eckart theorem, as it is usually described. The 'physical' part of the Wigner-Eckart theorem is given by the reduced matrix element of Equation 41. The reduced matrix element has no free lines and decomposes into products of Wigner 3nj symbols, as exemplified by Equation 49 and Figure 9. An example of the decomposition process for the graphical proof of Equation 8 is given in Appendix B.

8 Hamiltonian GUI

One of the goals of this work is to provide a useful tool for constructing model Hamiltonians from a pre-defined palette of nodes that may be used in a drag and drop fashion, such that the connections among different spin tensors are clearly displayed. It is also desirable to have a means to interface the computation of the Hamiltonian with, *e.g.*, molecular dynamics or visualization packages.

The molecular graphics lab[28] at the Scripps Research Institute has developed a suite of software tools that goes a long way towards accomplishing this goal. In particular, the vision package[29] allows one to construct networks of nodes, representing, *e.g.*, a particular contribution to the Hamiltonian. The output of the nodal network can be a numerical result that is incorporated into a matrix representation of the spin Hamiltonian or written to a file for subsequent use. The user may customize the nodes in vision to perform intermediate calculations or otherwise extend the basic set of nodes that are delivered in the distribution. Figure 13 demonstrates how this works in practice. Figure 13 is a low-level network in which many of the 'moving parts' are visible. Using the vision package, one may incorporate sub-networks into macros in order to achieve the high level of abstraction represented by, *e.g.*, Figure 9.

9 Matrix Elements of the Stochastic Liouville Equation

The Stochastic Liouville Equation (SLE) provides a means for rigorously treating spatial and spin degrees of freedom coupled by rotational diffusion.[30, 31] For the SLE formalism, basis vectors consist of a direct product of rotational diffusion operator eigenfunctions, typically linear combinations of $\{\mathfrak{D}^L_{KM}(\Omega)\}$, and $\{\mathcal{Q}\}$ operators. The relevant equation of motion is

$$\frac{\partial \sigma}{\partial t} = \left(-i\mathcal{H}^{\times} - \Gamma\right)\sigma, \tag{81}$$

where Γ is a superoperator describing the rotational diffusion and σ is a direct product of spin multipole operators and linear combinations of $\{\mathfrak{D}^L_{KM}(\Omega)\}$. Integration over the spatial degrees of freedom and a trace over the spin degrees of freedom allows to determine matrix elements of the SLE, Equation 81. The spin degrees of freedom may be handled by the methods of Section 6. Integration over the spatial degrees of freedom lead to classical normalization integrals for the

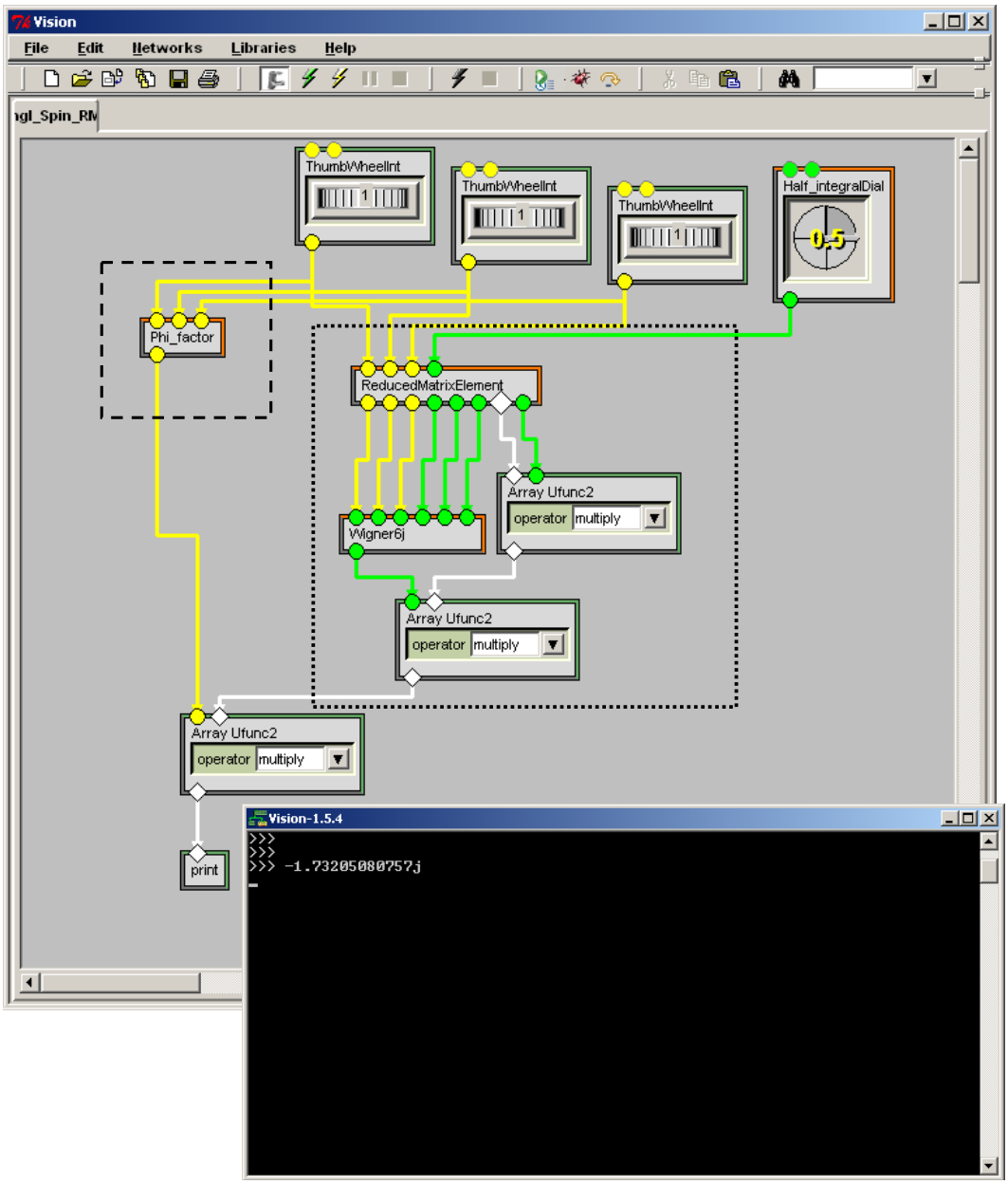

Figure 13: Demonstration of the use of the MGL vision package to compute reduced matrix elements of spin multipole operators à la Equation 51. The reduced matrix element is shown enclosed in the heavy dotted line. The nodes in the enclosed subnetwork are user defined nodes that compute the phase factor and weights for a given set of angular momentum values, as well as the needed Wigner 6j symbol. This calculation also shows the node for computing the necessary phase of spin multipole superoperator matrix elelments in heavy dashed lines. The numerical value of the reduced matrix element is shown in the python interactive shell.

$\{\mathfrak{D}^L_{KM}(\Omega)\}$ and integrals over products of three $\mathfrak{D}^L_{KM}(\Omega)$, which may be written in invariant form

$$\int \mathfrak{D}^{L_1}_{K_1M_1}(\Omega)\mathfrak{D}^{L_2}_{K_2M_2}(\Omega)\mathfrak{D}^{L_3}_{K_3M_3}(\Omega)\,d\Omega = 8\pi^2 \begin{pmatrix} L_1 & L_2 & L_3 \\ K_1 & K_2 & K_3 \end{pmatrix} \begin{pmatrix} L_1 & L_2 & L_3 \\ M_1 & M_2 & M_3 \end{pmatrix} \tag{82}$$

In this way the process of computing matrix elements of the Hamiltonian operator and the SLE reduces to the evaluation of invariant quantities.

10 Discussion

References

[1] Pyper, N. C. "Theory of symmetry in nuclear magnetic relaxation including applications to high resolution N.M.R. line shapes" *Mol. Phys.* 21:1–33 (1971).

[2] Meirovitch, E., D. Igner, E. Igner, G. Moro and J. H. Freed. "Electron-spin relaxation and ordering in smectic and supercooled nematic liquid crystals", *J. Chem. Phys.* 77:3915–3938 (1982).

[3] Earle, K. A., and Smirnov A. I. "High Field ESR: Applications to Protein Structure and Dynamics", *in* Biological Magnetic Resonance (O. Grinberg and L. J. Berliner, Eds.) 22 Chapter 4 (Kluwer Academic/Plenum Publishers, New York) 2004.

[4] Earle, K. A. and D. E. Budil "Calculating Slow-Motion ESR Spectra of Spin-Labeled Polymers" in "Advanced ESR Methods in Polymer Research", S. Schlick, Ed. (Wiley, New York) 2006.

[5] Lee, S., D. E. Budil and J. H. Freed. "Theory of two-dimensional Fourier transform electron spin resonance for ordered and viscous fluids", *J. Chem. Phys.* 101:5529–5558 (1994).

[6] Sanctuary, B. C. and T. K. Halstead. "Multipole NMR" *in* "Advances in Magnetic and Optical Resonance", W. S. Warren, Ed., v. 15, c. 3 (Academic, New York) 1990.

[7] Racah, G. "Theory of Complex Spectra. I" *Phys. Rev.* 61:186–197 (1942); Racah, G. "Theory of Complex Spectra. II" *Phys. Rev.* 62:438–462 (1942); Racah, G. "Theory of Complex Spectra. III" *Phys. Rev.* 63:367–382 (1943); Racah, G. "Theory of Complex Spectra. IV" *Phys. Rev.* 76:1352–1365 (1949).

[8] Judd, B. R. "Operator Techniques in Atomic Spectroscopy" (McGraw-Hill, New York) 1963.

[9] Blum, K. "Density Matrix Theory and Applications" (Plenum, New York) 1981.

[10] Jucys, A. P., I. Levinson and V. Vanagas. "Mathematical Apparatus of the Theory of Angular Momentum" (Israel Program for Scientific Translation, Jerusalem) 1962.

[11] El Baz, E. and B. Castel "Graphical Methods of Spin Algebras" Theoretical Physics, v. 2, (Marcel Dekker, New York) 1972.

[12] Danos, M. "Fully Consistent Phase Conventions in Angular Momentum Theory" *Ann. Phys.* 63:319–334 (1971).

[13] Brink, D. M. and G. R. Satchler. "Angular Momentum", third edition, (Clarendon, Oxford) 1993.

[14] Fano, U. and G. Racah "Irreducible Tensorial Sets" (Academic, New York) 1959.

[15] Silver, B. L. "Irreducible Tensor Methods: an Introduction for Chemists" (Academic Press, New York) 1976.

[16] Nakahara, M. "Geometry, Topology and Physics" (Institute of Physics, Bristol) 1990.

[17] Lehman, D. R. and J. S. O'Connell. "Graphical Recoupling of Angular Momenta" NBS Monograph 136 (U.S. Dept. of Commerce, Washington, D.C.) 1973.

[18] Danos, M. and V. Gillet "Angular Momentum Calculus in Quantum Physics" (World Scientific, Singapore) 1990.

[19] Lai, S-T. "Computation of Algebraic Formulas for Wigner 3-j, 6-j and 9-j Symbols by Maple" *International Journal of Quantum Chemistry* 52:593–607 (1994).

[20] http://www.rit.albany.edu/earlelab

[21] Biedenharn, L. C., and J. D. Louck. "Angular Momentum in Quantum Mechanics" *Encyclopedia of Mathematics and its Applications* v. 8 (Addison-Wesley, Reading) 1981.

[22] Biedenharn, L. C., and J. D. Louck. "The Racah-Wigner Algebra in Quantum Theory" *Encyclopedia of Mathematics and its Applications* v. 9 (Addison-Wesley, Reading) 1981.

[23] Edmonds, A. R. "Angular Momentum in Quantum Mechanics" (Princeton University Press, New York) second edition, 1960; third printing, with corrections, 1974. N.B. When using Edmonds, it is important to note that early editions and printings have significant errors.

[24] Benetis, N. P. "Spin-Lattice Relaxation of Ligand Nuclei in Slowly Reorienting Paramagnetic Complexes in the Electronic Doublet Spin State ($S = 1/2$). A Theoretical Approach for Strongly Coupled Two-Spin Systems", *J. Magn. Reson.* 68:469–489 (1986).

[25] Kruk, D. "Theory of Evolution and Relaxation of Multi-Spin Systems: Application to Nuclear Magnetic Resonance and Electron Spin Resonance" (Arima, Bury St. Edmunds) 2008.

[26] Borbat, P. P. and J. H. Freed. "Double-Quantum ESR and Distance Measurements" *in* "Distance Measurements in Biological Systems by EPR" *Biological Magnetic Resonance*, L. J. Berliner, S. S. Eaton, and G. R. Eaton, Eds.: v. 19, c. 9 Kluwer Academic/Plenum Publishers (New York, 2000), and references therein.

[27] Jeschke, G., and A. Schweiger. "Principles of pulse electron paramagnetic resonance" Clarendon Press (Oxford, 2001) and references therein.

[28] http://mgltools.scripps.edu/

[29] http://mgltools.scripps.edu/packages/vision

[30] Schneider, D. J., and J. H. Freed. "Calculating Slow Motional Magnetic Resonance Spectra: A User's Guide" *in* "Biological Magnetic Resonance" L. J. Berliner and J. Reuben, Eds. (Plenum, New York) 1989.

[31] Schneider, D. J. and J. H. Freed. "Spin Relaxation and Motional Dynamics" *in* "Lasers, Molecules and Methods" J. O. Hirschfelder, R. E. Wyatt, and R. D. Coalson, Eds. *Adv. Chem. Phys.* v. 73, c. 10, (1989).

[32] Benetis, N. P. "Theory for Dynamic Lineshapes of Strongly Correlated Two-Spin Systems" *J. Magn. Reson.* 85:275–293 (1989).

[33] Lindgard P.-A. "Tables of products of tensor operators and Stevens operators" *J. Phys. C: Solid State Phys.* 8:3401–3407 (1975).

[34] Zare, R. N. "Angular Momentum: Understanding Spatial Aspects in Chemistry and Physics" (Wiley, NY) 1986.

A Recoupling Coefficients

This appendix reproduces the results of Danos and Gillet[18] for recoupling coefficients with one, two or three zeroes. These results are particularly useful for comparing expressions derived with Danos' invariant graph technique to expressions derived via conventional means. Note that recoupling boxes are invariant under the interchange of the first two rows *and* the first two columns. The recoupling boxes are also invariant under reflection through both diagonals. Table 1 gives recoupling coefficients with one zero.

Table 2 gives recoupling coefficients with two zeroes. As noted by Danos and Gillet[18], these quantities have simple expressions in terms of a non-trivial phase and appropriate amplitudes.

Table 3 gives recoupling coefficients with three zeroes. The entries in Tables 2 and 3 allow considerable analytical simplifications of Danos diagrams. Danos and Gillet [18] recommend against the use of the results presented in Table 1. However, their use is so handy when comparing results with equivalent expressions in the literature, that this author dissents from Danos and Gillet's proscription.

$$
\begin{bmatrix} e & f & b \\ c & d & b \\ a & a & 0 \end{bmatrix} = \begin{bmatrix} e & c & a \\ f & d & a \\ b & b & 0 \end{bmatrix} = (-)^{f+c+a+b}\hat{a}\hat{b}\begin{Bmatrix} e & f & b \\ d & c & a \end{Bmatrix}
$$

$$
\begin{bmatrix} 0 & a & a \\ b & d & c \\ b & f & e \end{bmatrix} = \begin{bmatrix} d & b & c \\ a & 0 & a \\ f & b & e \end{bmatrix} = (-)^{f+c+a+b}\hat{f}\hat{c}\begin{Bmatrix} e & f & b \\ d & c & a \end{Bmatrix}
$$

$$
\begin{bmatrix} b & d & c \\ 0 & a & a \\ b & f & e \end{bmatrix} = \begin{bmatrix} a & 0 & a \\ d & b & c \\ f & b & e \end{bmatrix} = (-)^{e+d+a+b}\hat{f}\hat{c}\begin{Bmatrix} e & f & b \\ d & c & a \end{Bmatrix}
$$

$$
\begin{bmatrix} a & a & 0 \\ e & f & b \\ c & d & b \end{bmatrix} = \begin{bmatrix} a & e & c \\ a & f & d \\ 0 & b & b \end{bmatrix} = (-)^{f+c+a+b}\frac{\hat{c}\hat{d}}{\hat{a}}\begin{Bmatrix} e & f & b \\ d & c & a \end{Bmatrix}
$$

$$
\begin{bmatrix} e & f & b \\ a & a & 0 \\ c & d & b \end{bmatrix} = \begin{bmatrix} e & a & c \\ f & a & d \\ b & 0 & b \end{bmatrix} = (-)^{e+d+a+b}\frac{\hat{c}\hat{d}}{\hat{a}}\begin{Bmatrix} e & f & b \\ d & c & a \end{Bmatrix}
$$

Table 1: Recoupling coefficients with one zero expressed in terms of a Wigner 6j symbol, a phase and appropriate amplitudes.

$$\begin{bmatrix} e & 0 & e \\ 0 & f & f \\ e & f & b \end{bmatrix} = \begin{bmatrix} e & 0 & e \\ b & f & e \\ f & f & 0 \end{bmatrix} = \begin{bmatrix} e & b & f \\ 0 & f & f \\ e & e & 0 \end{bmatrix} = 1$$

$$\begin{bmatrix} 0 & e & e \\ f & 0 & f \\ f & e & b \end{bmatrix} = \begin{bmatrix} 0 & e & e \\ f & b & e \\ f & f & 0 \end{bmatrix} = \begin{bmatrix} b & e & f \\ f & 0 & f \\ e & e & 0 \end{bmatrix} = (-)^{e+f-b}$$

$$\begin{bmatrix} e & e & 0 \\ e & b & f \\ 0 & f & f \end{bmatrix} = \begin{bmatrix} b & e & f \\ e & e & 0 \\ f & 0 & f \end{bmatrix} = \frac{1}{\hat{e}\hat{e}}$$

$$\begin{bmatrix} e & e & 0 \\ b & e & f \\ f & 0 & f \end{bmatrix} = \begin{bmatrix} e & b & f \\ e & e & 0 \\ 0 & f & f \end{bmatrix} = \frac{(-)^{e+f-b}}{\hat{e}\hat{e}}$$

$$\begin{bmatrix} 0 & e & e \\ f & f & 0 \\ f & b & e \end{bmatrix} = \begin{bmatrix} 0 & f & f \\ e & f & b \\ e & 0 & e \end{bmatrix} = \begin{bmatrix} e & e & 0 \\ f & 0 & f \\ b & e & f \end{bmatrix} = \begin{bmatrix} e & f & b \\ e & 0 & e \\ 0 & f & f \end{bmatrix} = \frac{\hat{b}}{\hat{e}\hat{f}}$$

$$\begin{bmatrix} e & 0 & e \\ f & f & 0 \\ b & f & e \end{bmatrix} = \begin{bmatrix} e & f & b \\ 0 & f & f \\ e & 0 & e \end{bmatrix} = \begin{bmatrix} e & 0 & e \\ e & f & b \\ 0 & f & f \end{bmatrix} = \begin{bmatrix} e & e & 0 \\ 0 & f & f \\ e & b & f \end{bmatrix} = (-)^{e+f-b}\frac{\hat{b}}{\hat{e}\hat{f}}$$

Table 2: Recoupling coefficients with two zeroes expressed in terms of a phase and appropriate amplitudes.

$$\begin{bmatrix} e & f & b \\ 0 & 0 & 0 \\ e & f & b \end{bmatrix} = \begin{bmatrix} e & 0 & e \\ f & 0 & f \\ b & 0 & b \end{bmatrix} = \begin{bmatrix} 0 & 0 & 0 \\ e & f & b \\ e & f & b \end{bmatrix} = \begin{bmatrix} 0 & e & e \\ 0 & f & f \\ 0 & b & b \end{bmatrix} = 1$$

$$\begin{bmatrix} e & f & b \\ e & f & b \\ 0 & 0 & 0 \end{bmatrix} = \begin{bmatrix} e & e & 0 \\ f & f & 0 \\ b & b & 0 \end{bmatrix} = \frac{\hat{b}}{\hat{e}\hat{f}}$$

$$\begin{bmatrix} e & 0 & e \\ e & e & 0 \\ 0 & e & e \end{bmatrix} = \begin{bmatrix} e & e & 0 \\ 0 & e & e \\ e & 0 & e \end{bmatrix} = (-)^{2e}\frac{1}{\hat{e}\hat{e}}$$

$$\begin{bmatrix} e & e & 0 \\ e & 0 & e \\ 0 & e & e \end{bmatrix} = \begin{bmatrix} 0 & e & e \\ e & e & 0 \\ e & 0 & e \end{bmatrix} = \frac{1}{\hat{e}\hat{e}}$$

Table 3: Recoupling coefficients with three zeroes expressed in terms of a phase and appropriate amplitudes.

B Alternative Diagrammatic Proof of Equation 8

In order to compare the characteristics of Danos and Gillet's diagrammatic methods[18] of proof with those of Jucys, Levinson and Vanagas,[10] it is useful to rederive Equation 8 using the techniques of the latter. As these methods are better known than those of Danos and Gillet, only the most important steps will be discussed. However, on the general principle that 'two trivialities omitted is an impasse', many intermediate steps are left in, in order for neophytes to follow the diagram transformations. For more information on the diagrammatic techniques of Jucys and coworkers, consult the references.[10, 11, 13, 34] Some notes for those for whom the techniques of Jucys and coworkers are unknown may be helpful. The initial diagram is a Wigner 9j symbol. Each node represents a Wigner 3j symbol. The plus and minus signs determine the cyclic order in which the angular momenta are taken: a plus sign corresponds to a counterclockwise order; a minus sign corresponds to clockwise order. The direction of the arrow relative to a given node (incoming or outgoing) expresses the co- or contragredience of the associated angular momentum.

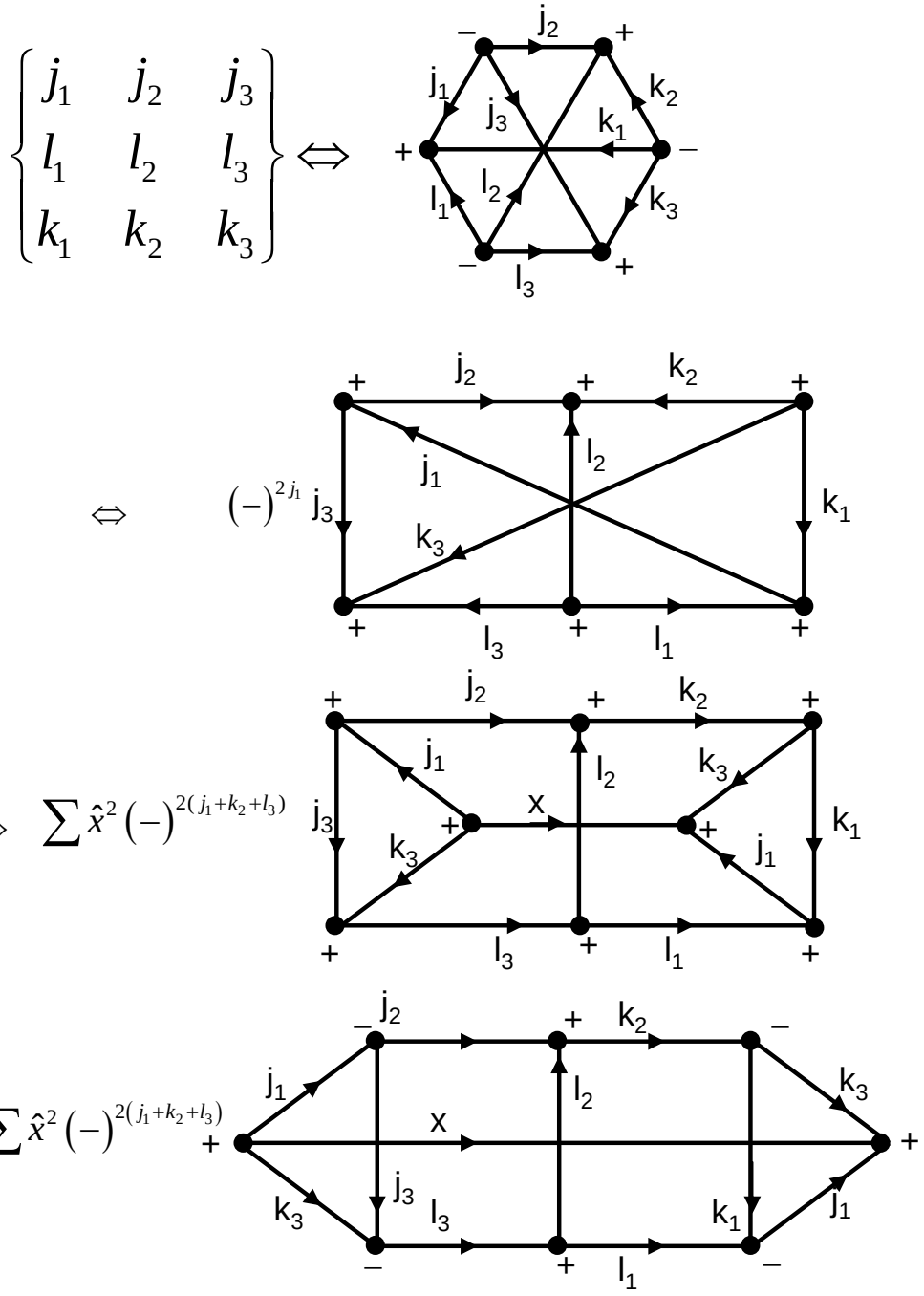

Figure 14: Equation 8 proved by the diagrammatic techniques of Jucys and coworkers.[10] All the steps up to separation over the internal lines are shown here. See the text for more details.

A 'closed' diagram, *i.e.* one with no lines that do not terminate in a node, represents a sum over all the azimuthal magnetic quantum numbers in the product of Wigner 3j symbols represented by the diagram.

Lines may be displaced and deformed at will, as long as the connections to the relevant nodes are maintained. In addition, the proper sign of each node must be accounted for. An example of this procedure is shown in the first transformation of the 9j symbol in Figure 14 where the nodes have been reordered for subsequent manipulation. If a positive node, say, is transformed so that two lines are exchanged relative to the third line associated with the node, corresponding to an odd permutation of the columns of a 3j symbol, then the sign of the node must be changed. Two similarly oriented lines can be transformed by the insertion of an identity operator. Since the identity may be written as the sum over azimuthal magnetic quantum numbers of a product of two Wigner 3j symbols, insertion of the identity will cause the number of nodes to increase. This transformation is also shown in Figure 14. If the direction of the line associated with angular momentum j is reversed, the diagram acquires a phase $(-)^{2j}$.

Another useful transformation of a Jucys diagram is to separate diagrams on parallel angular momentum lines. Three parallel lines may be joined and terminated in a Wigner 3j node. Thus, separation will also increase the number of nodes in the diagram. When this operation is performed, the resulting diagram represents the decomposition of the original sum over Wigner 3j symbols into independent products of sums over a *smaller* number of Wigner 3j symbols. Examples of this procedure are given in Figure 15. The most useful separations for the present purpose are those that reduce the diagram to products of sums over the magnetic azimuthal quantum numbers of 4 Wigner 3j symbols. Each such sum is equivalent to a Wigner 6j symbol. When reduced to this form, no intermediate azimuthal magnetic quantum numbers need be displayed in the final result. Figure 15 shows the various steps involved in manipulating the separated diagrams into the canonical form of a product of Wigner 6j symbols. Other authors transform the 6j diagrams into forms that look like tetrahedra. That this can be done is a fortuitous illustration of the group theoretic result that the symmetries of the Wigner 6j symbols are isomorphic to the symmetries of the tetrahedron. The symmetry group of the 9j symbol has no such felicitous representation.

There is one further point that should be emphasized. What Figure 15 does *not* show is the

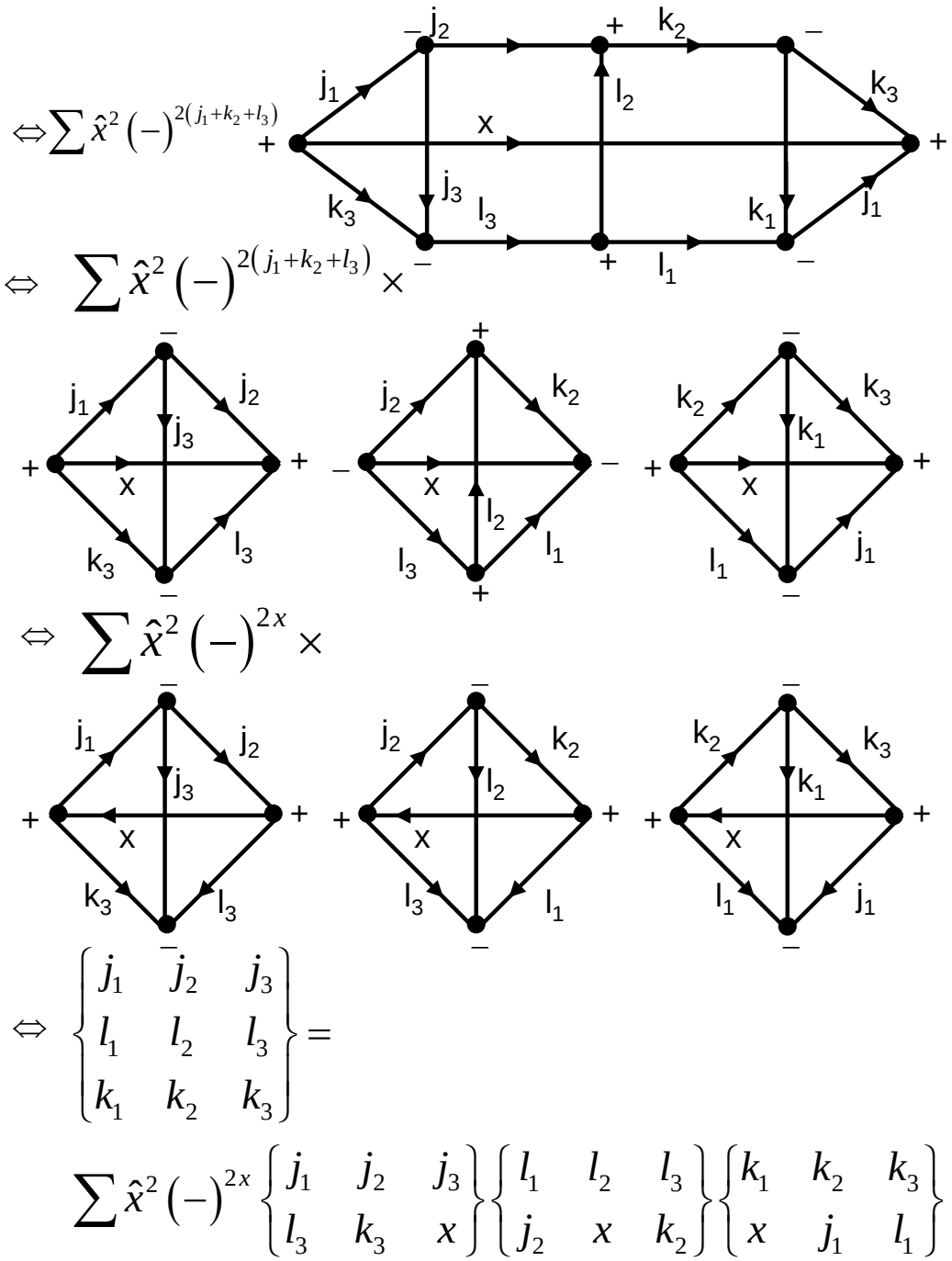

Figure 15: Final manipulations required to prove Equation 8 by the diagrammatic techniques of Jucys and coworkers.[10] The steps shown here indicate how one transforms subdiagrams into Wigner 6j symbols with the standard phase. See the text for more details.

ancillary calculations performed by the author to ensure that the phase of the final result was correct. In expert hands, this is presumably a quick exercise. In writing this particular graphical proof, which was the first non-trivial application of the Jucys diagrammatic technique attempted by the author, several tries were needed to get all of the details correct. An alternative graphical proof, quite similar to the one presented here, is given in El Baz and Castel, which does not contain as many intermediate steps as the current derivation.[11]

C Algebraic Proof of Equation 8

The power of the analytic method is that it is
much easier to discover things than to prove things.
—R. P. Feynman

For those readers for whom the graphical techniques reviewed here are unfamiliar or unconvincing, a final algebraic proof of Equation 8 is presented. In order to simplify the details of the calculation, some lesser known properties of Wigner 3j symbols will be exploited. These manipulations may make some of the graphical transformations in Figures 14 and 15 easier to understand. The usual transformation of a Clebsch-Gordan coefficient to a Wigner 3j symbol is given as follows:

$$(j_1\, j_2\, \alpha_1\, \alpha_2|\; j_3\, \alpha_3) = (-)^{j_1 - j_2 + \alpha_3} \hat{j}_3 \begin{pmatrix} j_1 & j_2 & j_3 \\ \alpha_1 & \alpha_2 & -\alpha_3 \end{pmatrix} \tag{83}$$

Although Equation 83 is useful and correct as far as it stands, the Wigner 3j symbol does not indicate clearly which angular momenta are the coupled angular momenta and which one is the resultant. This is a distinction that is very clear in the Clebsch-Gordan coefficient on the left hand side of Equation 83. There is a standard, although not well-known notation for Wigner 3j symbols, that allows one to track this distinction in angular momentum calculations. This is the covariant notation of Wigner, discussed in, *e.g.*, El Baz and Castel.[11] In this notation, Equation 83 may be written as follows

$$(j_1\, j_2\, \alpha_1\, \alpha_2|\; j_3\, \alpha_3) = (-)^{j_1 - j_2 + j_3} \hat{j}_3 \begin{pmatrix} j_1 & j_2 & \alpha_3 \\ \alpha_1 & \alpha_2 & j_3 \end{pmatrix}. \tag{84}$$

In this notation, the α_3 index is treated as a contragredient quantity. It may be related to cogredient quantities by the following prescription

$$\begin{pmatrix} j_1 & j_2 & j_3 \\ \alpha_1 & \alpha_2 & -\alpha_3 \end{pmatrix} = (-)^{j_3-\alpha_3} \begin{pmatrix} j_1 & j_2 & \alpha_3 \\ \alpha_1 & \alpha_2 & j_3 \end{pmatrix}. \tag{85}$$

Using the symmetry properties of Wigner 3j symbols, one has the following useful identity

$$\begin{pmatrix} j_1 & j_2 & j_3 \\ \alpha_1 & \alpha_2 & \alpha_3 \end{pmatrix} = \begin{pmatrix} \alpha_1 & \alpha_2 & \alpha_3 \\ j_1 & j_2 & j_3 \end{pmatrix}. \tag{86}$$

If one specifies that in products of Wigner 3j symbols expressed in covariant form that repeated indices where one of the indices is contragredient and one is cogredient are summed over, than one may use Equation 86 to express, *e.g.*, orthogonality relations for Wigner 3j symbols in a very compact form. For example

$$\sum_{m_1,m_2} \begin{pmatrix} j_1 & j_2 & j_3 \\ m_1 & m_2 & m_3 \end{pmatrix} \begin{pmatrix} j_1 & j_2 & j_3' \\ m_1 & m_2 & m_3' \end{pmatrix} = \begin{pmatrix} j_1 & j_2 & j_3 \\ m_1 & m_2 & m_3 \end{pmatrix} \begin{pmatrix} m_1 & m_2 & m_3' \\ j_1 & j_2 & j_3' \end{pmatrix} = \frac{\delta_{j_3,j_3'}\delta_{m_3,m_3'}}{\hat{j}_3^2}, \tag{87}$$

$$\sum_{j_3,m_3} \hat{j}_3^2 \begin{pmatrix} j_1 & j_2 & j_3 \\ m_1 & m_2 & m_3 \end{pmatrix} \begin{pmatrix} j_1 & j_2 & j_3 \\ m_1' & m_2' & m_3 \end{pmatrix} = \sum_{j_3,m_3} \hat{j}_3^2 \begin{pmatrix} j_1 & j_2 & j_3 \\ m_1 & m_2 & m_3 \end{pmatrix} \begin{pmatrix} m_1' & m_2' & m_3 \\ j_1 & j_2 & j_3 \end{pmatrix} = \delta_{m_1,m_1'}\delta_{m_2,m_2'} \tag{88}$$

If m_3 is summed over in Equation 87, then one has the following relation

$$\begin{pmatrix} j_1 & j_2 & j_3 \\ \alpha_1 & \alpha_2 & \alpha_3 \end{pmatrix} \begin{pmatrix} \alpha_1 & \alpha_2 & \alpha_3 \\ j_1 & j_2 & j_3 \end{pmatrix} = 1, \tag{89}$$

where the convention that one only sums over repeated *Greek* indices of different gredience is introduced. Equation 89 is the algebraic expression of the 'separation over three kinetic lines' shown in the second line of Figure 15.[11]

The identity expressed in Equation 87 is used to introduce an extra 'kinetic line' in the third line of Figure 14. In writing algebraic equivalents of Jucys diagrams, recall that each node of a

Jucys diagram corresponds to a Wigner 3j symbol. The gredience of each line may be recalled by the mnemonic: "Down and out". This means that a 'kinetic' line pointing *out* of a node has cogredient (in the Wigner sense) character. Thus, the azimuthal magnetic quantum number is in the lower or 'down' row. A contragredient line has an azimuthal quantum number that is in the upper row.

Using the covariant summation convention, an algebraic expression for the Wigner 6j symbol may be written down in quite compact form[11]

$$\left\{ \begin{array}{ccc} j_1 & j_2 & j_3 \\ l_1 & l_2 & l_3 \end{array} \right\} = \left(\begin{array}{ccc} j_1 & j_2 & \alpha_3 \\ \alpha_1 & \alpha_2 & j_3 \end{array} \right) \left(\begin{array}{ccc} \alpha_1 & l_2 & l_3 \\ j_1 & \beta_2 & \beta_3 \end{array} \right) \left(\begin{array}{ccc} l_1 & \beta_2 & j_3 \\ \beta_1 & l_2 & \alpha_1 \end{array} \right) \left(\begin{array}{ccc} \beta_1 & \alpha_2 & \beta_3 \\ l_1 & j_2 & l_3 \end{array} \right). \qquad (90)$$

Note that this definition of the Wigner 6j symbol does not have the cumbersome phase factors that are a necessary adjunct of the noncovariant notation of other authors.[13, 23, 34] The Wigner 9j symbol may also be defined covariantly as follows:[11]

$$\left\{ \begin{array}{ccc} j_1 & j_2 & j_3 \\ l_1 & l_2 & l_3 \\ k_1 & k_2 & k_3 \end{array} \right\} = \left(\begin{array}{ccc} j_1 & j_2 & j_3 \\ \mu_1 & \mu_2 & \mu_3 \end{array} \right) \left(\begin{array}{ccc} \mu_2 & \lambda_2 & \kappa_2 \\ j_2 & l_2 & k_2 \end{array} \right) \left(\begin{array}{ccc} k_1 & k_2 & k_3 \\ \kappa_1 & \kappa_2 & \kappa_3 \end{array} \right)$$
$$\left(\begin{array}{ccc} \kappa_3 & \mu_3 & \lambda_3 \\ k_3 & j_3 & l_3 \end{array} \right) \left(\begin{array}{ccc} l_3 & l_1 & l_2 \\ \lambda_3 & \lambda_1 & \lambda_2 \end{array} \right) \left(\begin{array}{ccc} \lambda_1 & \kappa_1 & \mu_1 \\ l_1 & k_1 & j_1 \end{array} \right) \qquad (91)$$

The transformations of the Wigner 9j symbol shown in Figure 15 may be written as follows

$$\left\{ \begin{array}{ccc} j_1 & j_2 & j_3 \\ l_1 & l_2 & l_3 \\ k_1 & k_2 & k_3 \end{array} \right\} = \sum_x \hat{x}^2 (-)^{2(j_1+k_2+l_3)} \times$$
$$\left(\begin{array}{ccc} -\mu_1 & j_2 & j_3 \\ j_1 & \mu_2 & \mu_3 \end{array} \right) \left(\begin{array}{ccc} \mu_2 & \lambda_2 & k_2 \\ j_2 & l_2 & -\kappa_2 \end{array} \right) \left(\begin{array}{ccc} k_1 & -\kappa_2 & k_3 \\ \kappa_1 & k_2 & \kappa_3 \end{array} \right)$$
$$\left(\begin{array}{ccc} \kappa_3 & \mu_3 & l_3 \\ k_3 & j_3 & -\lambda_3 \end{array} \right) \left(\begin{array}{ccc} -\lambda_3 & l_1 & l_2 \\ l_3 & \lambda_1 & \lambda_2 \end{array} \right) \left(\begin{array}{ccc} \lambda_1 & \kappa_1 & j_1 \\ l_1 & k_1 & -\mu_1 \end{array} \right)$$
$$\left(\begin{array}{ccc} j_1 & k_3 & x \\ -\mu_1 & -\kappa_3 & \xi \end{array} \right) \left(\begin{array}{ccc} \xi & -\mu_1 & -\kappa_3 \\ x & j_1 & k_3 \end{array} \right)$$

$$\begin{pmatrix} \mu_2 & \xi & -\lambda_3 \\ j_2 & x & l_3 \end{pmatrix} \begin{pmatrix} j_2 & x & l_3 \\ \mu_2 & \xi & -\lambda_3 \end{pmatrix} \begin{pmatrix} \lambda_1 & \xi & \kappa_2 \\ l_1 & x & k_2 \end{pmatrix} \begin{pmatrix} l_1 & x & k_2 \\ \lambda_1 & \xi & \kappa_2 \end{pmatrix} \tag{92}$$

Note that the azimuthal magnetic quantum numbers may be treated as dummy indices, given that they are all summed over. Due to the summation range, there is no further phase factor under the substitutions $-\mu_1 \rightarrow \mu_1$, etc. This operation will be done to facilitate further manipulations of Equation 92.

In order to separate out the products of Wigner 3j symbols corresponding to Wigner 6j symbols, one may regroup the order of terms in Equation 92. Once this has been done, four of the Wigner 3j symbols require an odd permutation of columns in order to bring them into the proper orientation for the standard definition of a Wigner 6j symbols. This process introduces a phase factor $(-)^{l_2+k_2+l_1}$, upon simplification. Finally, the gredience of several columns need to be changed in order to satisfy the standard definition of a Wigner 6j symbol. These gredience changes introduce a further phase factor $(-)^{2(3x+l_1+l_2+l_3+j_1)}$ and are the origin of the observation that changing the direction of a line with angular momentum j in a Jucys diagram introduces a phase $(-)^{2j}$. Using the observation that $2(l_1 + l_2 + l_3)$ must be an even integer and four times any individual index must be an even integer, the overall phase simplifies to $(-)^{2x}$. Once these operations have been done, the remaining products of Wigner 3j symbols differ from the definition given in Equation 90 by at most a cyclic permutation of columns in the Wigner 3j symbols, which does not affect the phase.

When these transformations have been made, one finds

$$\begin{Bmatrix} j_1 & j_2 & j_3 \\ l_1 & l_2 & l_3 \\ k_1 & k_2 & k_3 \end{Bmatrix} = \sum_x \hat{x}^2 (-)^{2x} \times$$

$$\sum_{\mu_1,\mu_2,\mu_3,\lambda_3,\kappa_3,\xi} \begin{pmatrix} j_1 & k_3 & \xi \\ \mu_1 & \kappa_3 & x \end{pmatrix} \begin{pmatrix} \mu_1 & j_2 & j_3 \\ j_1 & \mu_2 & \mu_3 \end{pmatrix} \begin{pmatrix} \mu_2 & x & l_3 \\ j_2 & \xi & \lambda_3 \end{pmatrix} \begin{pmatrix} \kappa_3 & \mu_3 & \lambda_3 \\ k_3 & j_3 & l_3 \end{pmatrix}$$

$$\sum_{\lambda_1,\lambda_2,\lambda_3,\mu_2,\xi,\kappa_2} \begin{pmatrix} j_2 & l_3 & \xi \\ \mu_2 & \lambda_3 & x \end{pmatrix} \begin{pmatrix} \mu_2 & k_2 & l_2 \\ j_2 & \kappa_2 & \lambda_2 \end{pmatrix} \begin{pmatrix} \kappa_2 & x & l_1 \\ k_2 & \xi & \lambda_1 \end{pmatrix} \begin{pmatrix} \lambda_3 & \lambda_2 & \lambda_1 \\ l_3 & l_2 & l_1 \end{pmatrix}$$

$$\sum_{\kappa_1,\kappa_2,\kappa_3,\xi,\mu_1,\lambda_1} \begin{pmatrix} k_2 & l_1 & \xi \\ \kappa_2 & \lambda_1 & x \end{pmatrix} \begin{pmatrix} \kappa_2 & k_3 & k_1 \\ k_2 & \kappa_3 & \kappa_1 \end{pmatrix} \begin{pmatrix} \kappa_3 & x & j_1 \\ k_3 & \xi & \mu_1 \end{pmatrix} \begin{pmatrix} \lambda_1 & \kappa_1 & \mu_1 \\ l_1 & k_1 & j_1 \end{pmatrix} \tag{93}$$

$$= \sum_x \hat{x}^2 (-)^{2x} \begin{Bmatrix} j_1 & k_3 & x \\ l_3 & j_2 & j_3 \end{Bmatrix} \begin{Bmatrix} j_2 & l_3 & x \\ l_1 & k_2 & l_2 \end{Bmatrix} \begin{Bmatrix} k_1 & k_2 & k_3 \\ x & j_1 & l_1 \end{Bmatrix}$$

$$= \sum_x \hat{x}^2 (-)^{2x} \begin{Bmatrix} j_1 & j_2 & j_3 \\ l_3 & k_3 & x \end{Bmatrix} \begin{Bmatrix} l_1 & l_2 & l_3 \\ j_2 & x & k_2 \end{Bmatrix} \begin{Bmatrix} k_1 & k_2 & k_3 \\ x & j_1 & l_1 \end{Bmatrix} \tag{94}$$

In writing Equation 93, use has been made of the Kronecker delta functions in Equations 87 and 88 to decompose the product into three independent products. The final form of Equation 94 was derived using the symmetry properties of the Wigner 6j symbols under permutations of columns and interchange of row entries in any two columns.